Effect of extrusion temperature and speed on texture evolution in Mg-Zn-Gd alloy and their correlation with mechanical properties

Shiyuan Xu¹, Jing Xu², Bo Guan^{2*}, Xuan Luo^{1*}, Dikai Guan³, Xuejian Li⁴, Huihui Yu², Jiahao Wang², Qiang Hu², Yunchang Xin^{1, 2*}

*Correspondence: Bo Guan, bguan2022@163.com;

Xuan Luo, luo.xuan@njtech.edu.cn Yunchang Xin, ycxin@njtech.edu.cn.

Abstract: In this study, the microstructure and mechanical properties of a Mg-2Zn-1Gd alloy (wt.%) at different extrusion speeds and temperatures were studied. The results demonstrated that rare earth Mg alloys (Mg-RE alloys) do not invariably result in the formation of RE textures, particularly during the high-speed (32 m/min) extrusion process. The texture characteristics of Mg-Re alloys after low-speed extrusion also exhibits a significant discrepancy with extrusion temperature. For rods extruded at 300 °C and 400 °C with an extrusion speed of 3.2 m/min and 32 m/min, decreasing the extrusion temperature and speed would promote the formation of RE texture. For rods extruded at 500 °C, strong basal textures are observed for the rods extruded with speed of 0.2 m/min, 3.2 m/min and 32 m/min. Further examination revealed that the formation of RE texture for rods extruded at lower temperature and speed is related to the segregation of solute atoms at grain boundaries, which would contribute to increase the critical strain for dynamic recrystallization, thus increasing the range of grain orientation after nucleation. However, for rods extruded at higher temperature and speed, the activation of basal slips in the recrystallized grains plays an important role on the formation of strong basal texture. In addition, the effect of microstructure

 $^{^{\}rm 1}$ Key Laboratory for Light-weight Materials, Nanjing Tech University, Nanjing $210009, {\rm China}$

² Institute of Applied Physics, Jiangxi Academy of Sciences, Nanchang, 330029, China

³ Department of Mechanical Engineering, University of Southampton, Southampton, SO171BJ, UK

⁴ National Key Laboratory of Precision Hot Processing of Metal, Harbin Institute of Technology, Harbin 150001, China

evolution with extrusion parameters on mechanical properties of Mg-2Zn-1Gd rods are also systematically investigated, and a numerical calculation are conducted to determine the mechanism on the effect of texture evolution on mechanical properties.

Key words: Mg-RE alloys; Texture; High-speed extrusion; Dynamic recrystallization

1. Introduction

Mg is comprising 2.7% of the earth's crust, and it can be commercially produced from its ore or the seawater [1-3]. Mg alloys have the lowest density of all structural metals, with a density of approximately 1.8 g/cm³. This is approximately 25% of the density of steel and 75% of the density of Al alloys. Furthermore, Mg alloys possess the excellent thermal conductivity [4], significant vibration damping [5], and good electromagnetic shielding property [6]. These unique features render Mg alloys highly in the aerospace [7] and automotive industries [8], 3C products [9, 10]. However, the inherent limitations of Mg alloys, including their low strength [11] and limited plasticity at room temperature [12], impose constraints on their practical applications [13].

In general, thermomechanical-processed products of conventional Mg alloys have strong basal texture [14]. In the case of rolled sheets or extruded rods of AZ31 Mg alloys [15], the strong basal texture corresponds to the c-axis, which is parallel to the normal direction of the plates or the extrusion direction of the rods [16, 17]. The strong texture generally results in unsatisfactory formability of Mg alloys [18]. The trace addition of rare earth (RE) elements is found to effectively modify the texture [19], leading to the formation of RE texture, which is commonly referred to a $<11\overline{2}1>$ component being parallel to ED for an extruded product. It is considered that the RE texture poses a significant effect on the improvement of ductility [20]. For example, Mishra et al. [21, 22] investigated the effect of Ce addition on the microstructure and mechanical properties of Mg alloy. Comparing to pure Mg, the addition of 0.5 wt.% Ce could effectively improve the tensile ductility from 9.1% to 31%. The results of the microstructure examination demonstrated that the enhanced tensile ductility is essentially related to the random texture of Mg-0.5 wt.% Ce, that is, the maximum texture strength of the extruded Mg rod is 7.4 mrd (multiples of random distribution), and that of the Mg-0.5 wt.% Ce rod is about 3.3 mrd. Lee et al. [23] studied the effect of Gd addition on microstructure and mechanical properties of Mg alloys. It was found that compared with pure Mg, the maximum texture strength of extruded Mg-5Gd rods decreased from 11.6 mrd to 5.9 mrd, and the elongation increased from 5.8 % to 22.3 %. Stanford et al. [24] carefully examined the texture and mechanical properties of five binary Mg-based alloys, including Mg-0.99 wt.% Al, Mg-1.87 wt.% Sn, Mg-0.1 wt.% Ca, Mg-0.22 wt.% La and Mg-1.55 wt.% Gd. It is reported that Mg-La and Mg-Gd alloys exhibit the best ductility due to the weak extrusion texture, where the grain size of these binary alloys is comparable. In particular, the addition of Gd promotes the formation of Re texture component with $<11\overline{2}1>$ direction being parallel to ED. Due to the favorable effect of Gd addition on mechanical properties, a series of Mg-Zn-Gd alloys with weakened basal texture have been developed in recent years, and parts of Mg-Zn-Gd alloys can exhibit high ductility of about 45%.

For Mg alloys, extrusion is considered to be an important plastic-processing method [25]. However, the extrusion speeds of Mg alloys are reported to be much lower than those of Al alloys, which significantly increase the manufacturing costs of Mg products [26]. For example, the extrusion speed of 1350 Al alloy and 6063 Al alloy could be as high as 100 m/min and 60 m/min, respectively. However, the maximum extrusion speeds of Mg-6Zn-0.5Zr (wt.%, ZK60) and Mg-3Al-1Zn-0.3Mn (wt.%, AZ31) are approximately 4 m/min and 24 m/min, respectively [27, 28]. The processing cost of Mg alloys would be more than 3 times higher than that of Al alloys, when the same extruded products are considered. Therefore, increasing the extrusion speed of Mg alloys is of great importance to expand the application of Mg alloy products [29]. Jiang et al. [2] reported that the Mg-1.58Zn-0.52Gd (wt.%) alloy could be successfully extruded at 60 m/min at 300 °C without any surface defects due to the enhanced ductility, and the extruded rod of Mg-1.58Zn-0.52Gd (wt.%) alloy exhibits a high tensile ductility of about 30%, due to the formation of RE texture at the position between $<2\overline{1}14>$ and $<2\overline{1}\overline{1}2>$ parallel to ED. A question arises considering the following reasons, can the RE texture always exists in Mg-RE alloys, especially for Mg-RE alloys after high-speed extrusion? It is considered that the formation of RE texture component is related to shear bands or boundary segregation. However, both the formation of shear band or segregation solute atoms at boundaries would be suppressed at higher temperature [30, 31]. Consequently, the formation of RE texture would be suppressed at higher temperature [32]. For example, N. Stanford et al. reported that a RE texture component is dominant for Mg-1.55 wt.% Gd alloys extruded at temperatures lower than 500 °C,

while a conventional basal texture is dominant at temperature higher than 500 °C [24]. However, it is also reported that higher extrusion temperatures could lead to a weaker texture. Zegine et al. [33] found that the texture strength of Mg-6Zn-0.5Zr-xLa (at.%) alloys decreased from 22 mrd to 21 mrd when extruded at extrusion temperatures of 300 °C and 400 °C. It is considered that an increase in temperature promotes dynamic recrystallisation during the extrusion process, leading to a more random grain orientation. Zhang et al. [34] investigated the microstructure evolution in AZ31 sheets at temperatures of 350 °C, 400 °C, and 450 °C. The results indicated that the texture strength decreased from 18.3 mrd to 15.8 mrd, as increasing the temperature from 350 °C to 450 °C.

In order to reveal the texture evolution with extrusion conditions and its effect on mechanical properties of Mg-RE alloys. The microstructure evolution and mechanical properties of Mg-2Zn-1Gd alloy with extrusion temperatures within the range of 300-500 °C and extrusion speeds within the range of 0.2-32 m/min of Mg-2Zn-1Gd alloy were carefully examined. Firstly, the mechanism on the variation of texture with extrusion temperature and speed in extruded Mg-Re alloys was enclosed. Then, a numerical calculation was conducted to determine the mechanism on the effect of texture evolution on mechanical properties.

2. Experimental

2.1. Materials preparation

The as-cast Mg-2Zn-1Gd (wt.%) ingot was cut into cylindrical samples with a diameter of 35 mm and a height of 70 mm, and then homogenized at 450 °C for 6 h. The homogenized samples then extruded into rods with a diameter of 6 mm at temperatures of 300, 400, and 500 °C, and speeds of 0.2, 3.2, and 32 m/min, respectively. Designations of these rods are given in Table 1.

Table 1. Designations of rods with 9 different extrusion conditions.

Number	Extrusion Conditions	Designations
Rod 1	Temperate: 300 °C; Speed: 0.2 m/min.	300 °C 0.2 m/min

Rod 2	Temperate: 300 °C;	Speed: 3.2 m/min.	300 °C 3.2 m/min
Rod 3	Temperate: 300 °C;	Speed: 32 m/min.	300 °C 32 m/min
Rod 4	Temperate: 400 °C;	Speed: 0.2 m/min.	400 °C 0.2 m/min
Rod 5	Temperate: 400 °C;	Speed: 3.2 m/min.	400 °C 3.2 m/min
Rod 6	Temperate: 400 °C;	Speed: 32 m/min.	400 °C 32 m/min
Rod 7	Temperate: 500 °C;	Speed: 0.2 m/min.	500 °C 0.2 m/min
Rod 8	Temperate: 500 °C;	Speed: 3.2 m/min.	500 °C 3.2 m/min
Rod 9	Temperate: 500 °C;	Speed: 32 m/min.	500 °C 32 m/min

2.2. Mechanical testing

Uniaxial tensile and compression tests were performed along the extrusion direction (ED) using an MTS testing machine (20 kN) at room temperature, with a loading rate of 0.6 mm/min. The specimens used for tensile test were dog-bone-shaped with a gauge length of 10 mm, width of 2 mm, and thickness of 1.5 mm. The plastic strain was measured using an extensometer during the tensile testing. The samples used for the compression tests were cylinders with a diameter of 6 mm and height of 9 mm. Tensile/compressive yield strength, ultimate tensile/compressive strength and elongation to fracture are the average values of at least three individually repeated tests. In order to prevent slipping during the testing process and causing experimental failure, all samples were ground to 1000 grit with SiC sandpaper.

2.3. Microstructural examination

Microstructure was investigated by electron backscatter diffraction (EBSD) using a scanning electron microscope (SEM, TESCAN MIRA4) equipped with an AZtec system. The samples used for the EBSD measurements were mechanically ground and then electrochemically polished at 20 V using an electrolyte containing 90% ethanol and 10% perchloric acid. When characterizing the grain structure, the calibration area of EBSD scanning is usually set to 500 $\mu m \times 500 \ \mu m$, and the step size is 1 μm . However, when the extrusion speed is 0.2 m/min and the extrusion temperature is 300 °C and

400 °C, the calibration area is adjusted to 300 μ m × 300 μ m due to the fine grain size, and the step size is reduced to 0.3 μ m to capture the details of the grain structure more accurately. EBSD data were analyzed by AZtec Crystal software to obtain the size distribution of fully recrystallized grains and grain boundary misorientation angle (GBMA). The GBMA reflects the orientation relationship between grains and grain boundaries: low-angle grain boundaries (LAGBs, 2° < GBMA < 10°) can impede dislocation slip, thereby strengthening the alloy, and high-angle grain boundaries (HAGBs, GBMA > 10°) can also enhance material strength, as their higher interfacial energy enables a more effective obstruction of dislocation motion.

The microstructure of the extruded rod at extrusion temperature of 300, 400 and 500 °C, and extrusion speed of 0.2 m/min were further investigated by transmission electron microscopy (TEM, FEI Tecnai F20, 200 kV). Firstly, the TEM observation sample was carefully ground to make a thin sheet with a thickness of about 100 μ m, and then the double spray test was carried out. The double spray tests parameters were 78 V voltage, -47 °C temperature, 8 photosensitive value and 17 liquid pump flow rate.

3. Results

3.1. Microstructures of extruded Mg-2Zn-1Gd rods

Fig. 1 shows the Inverse pole figure (IPF) maps of the extruded rods. From Fig. 1(a), at extrusion temperature of 300 °C, part of the deformed grains with large size could be observed for sample extruded with speed of 0.2 m/min. With the increase of extrusion speed, the rod is completely recrystallized at 3.2 m/min, then obvious grain growth is observed at 32 m/min. At the extrusion temperature of 400 °C with speed of 0.2 m/min (Fig. 1(d)), the sample is partially recrystallized, and the heterogeneous microstructures containing both the coarse-deformed grains and the fine-recrystallized grains are observed. With increasing the extrusion temperature and speed, the grains become fully recrystallized, and a higher extrusion temperature or a higher extrusion speed would promote the formation of grains with lager size. It is noted that the grain orientations change noticeably with extrusion temperature and speed. At both the extrusion temperature of 300 °C and 400 °C with a speed of 0.2 m/min, the deformed

grains are oriented with $<10\overline{1}0>$ orientation being parallel to the extrusion direction (ED). At the extrusion temperature of 300 °C with a speed of 3.2 m/min, grains with the $<10\overline{1}0>$ orientation and $<1\overline{2}10>$ orientation being parallel to ED and RE texture with orientation being a position between $<11\overline{2}0>$ and <0001> are all observed. With increasing the extrusion temperature and extrusion speed, the frequency of grains of RE texture decrease. For the sample extruded at 400 °C with extrusion speed of 32 m/min and all the samples extruded at 500 °C, RE texture could hardly been observed.

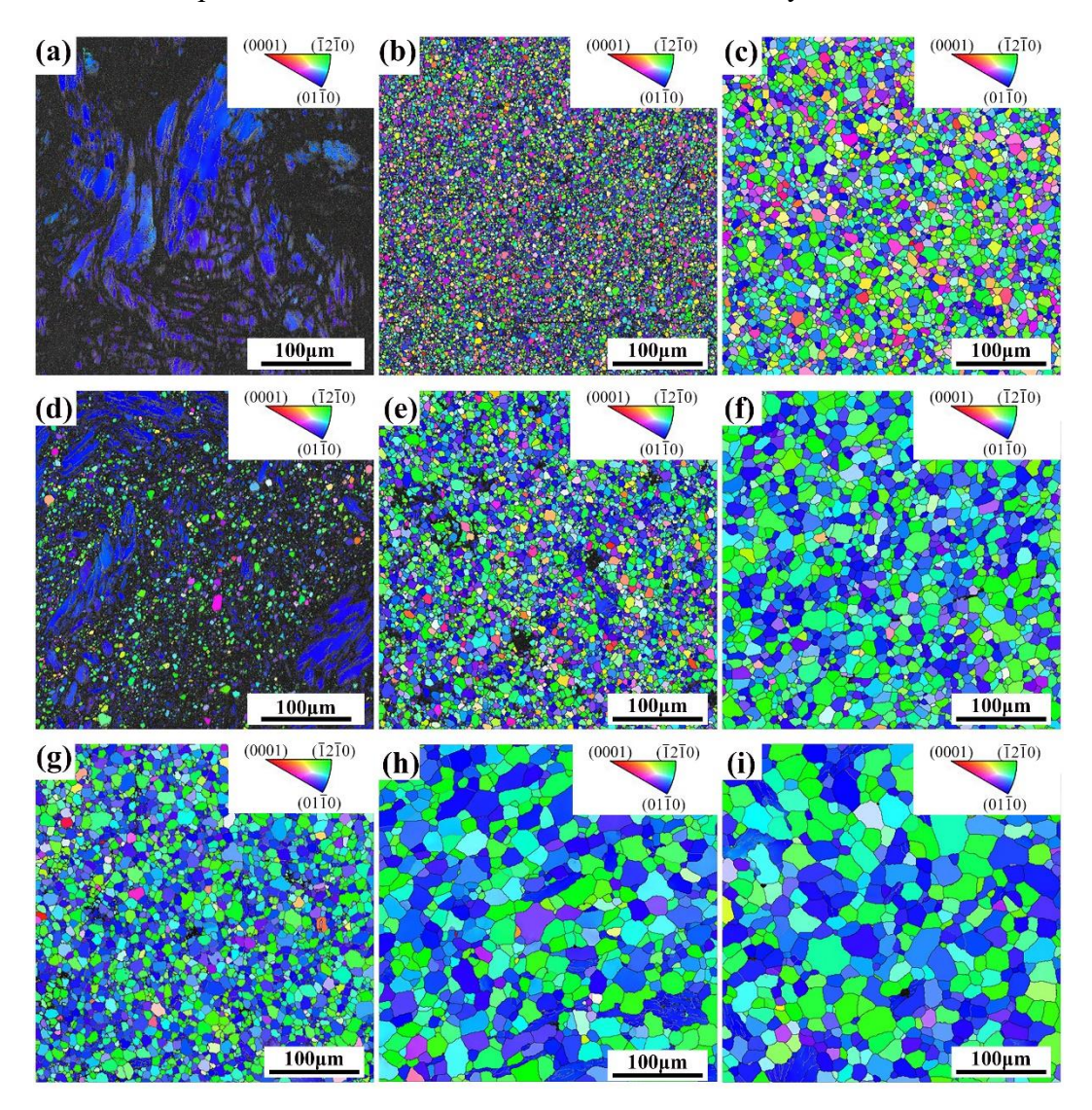


Fig. 1. Microstructure evolution of extruded Mg-2Zn-1Gd (wt.%) rod under extrusion conditions: (a) 300 °C 0.2 m/min, (b) 300 °C 3.2 m/min, (c) 300 °C 32 m/min, (d) 400 °C 0.2 m/min, (e) 400 °C 3.2 m/min, (f) 400 °C 32 m/min, (g) 500 °C 0.2 m/min, (h) 500 °C 3.2 m/min, (i) 500 °C 32 m/min along the ED of IPF maps.

Due to the lower index rate in the IPF maps of rods extruded at 300 °C and 400 °C with speed of 0.2 m/min. The microstructure of those rods were further investigated by transmission electron microscopy (TEM), as shown in Figs. 2 and 3. For comparison, the microstructure of rods extruded with speed of 0.2 m/min at 500 °C was also characterized by TEM, which are shown in Fig. 4. Both the deformed grains with high-density dislocations (Fig. 2 (a)) and fine recrystallized grains with low-density dislocations (Fig. 2 (b)) were observed in rod extruded at 300 °C with extrusion speed of 0.2 m/min. High-density dislocations can also be observed of the rod extruded at 400 °C, while the dislocation density is lower than that of rod extruded at 300 °C (Fig. 3 (a)). In addition, it can be seen from Fig. 3 (b) that the grain size of recrystallized grain is significantly larger than that of 300 °C 0.2 m/min. As the extrusion temperature increases to 500 °C, the grain size becomes larger, and the dislocation density in the recrystallized grains are significantly lower than that of rods extruded at 300 °C and 400 °C.

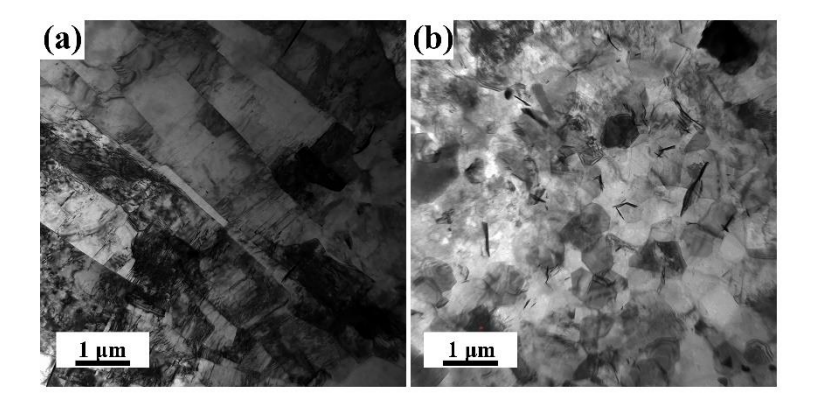


Fig. 2. TEM images of Mg-2Zn-1Gd (wt.%) rod extruded at 300 °C with speed of 0.2 m/min of (a) deformed regions and (b) recrystallized regions.

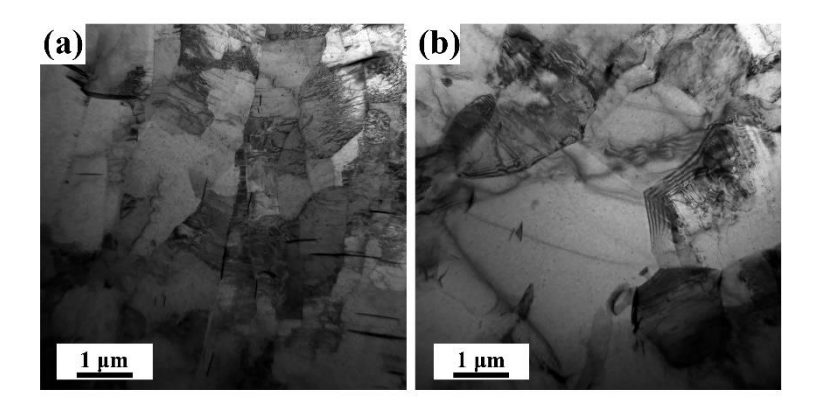


Fig. 3. TEM images of Mg-2Zn-1Gd (wt.%) rod extruded at 400 °C with speed of 0.2 m/min of (a) deformed regions and (b) recrystallized regions.

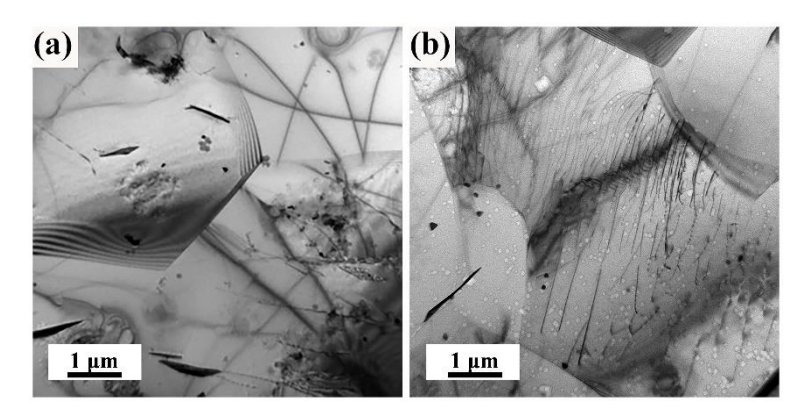


Fig. 4. TEM images of Mg-2Zn-1Gd (wt.%) rod extruded at 500 °C with speed of 0.2 m/min of (a-b) recrystallized regions.

In order to quantitatively analyze the microstructure evolution, the average grain size of recrystallized grains was analyzed. From Fig. 1, most of the coarsely deformed grains are observed at 300 °C 0.2 m/min and 400 °C 0.2 m/min, and it is difficult to accurately determine the average grain size in these samples based on the IPF images. Therefore, for the rods extruded at 300 °C and 400 °C with speed of 0.2 m/min, the grain diameters of the recrystallized grains of the two rods were measured based on the TEM images, and that of the other rods were measured based on the IPF images. For all the rods, more than 500 grains were used to analyze the average grain size. From Fig. 5, the average grain size of the rod increases with increasing the extrusion temperature and extrusion speed. At the extrusion temperature of 300 °C, the average grain size for the recrystallized grains is about 0.37 µm for rod extruded with a speed of 0.2 m/min. When the extrusion speed is 3.2 m/min and 32 m/min, the grains are in a completely recrystallized state, and the average grain size reaches 4.75 and 8.87 µm, respectively. When the extrusion temperature increases to 400 °C, the average grain sizes are 0.7 µm, 7.04 µm and 12.64 µm at the extrusion speeds of 0.2 m/min, 3.2 m/min and 32 m/min, respectively. When the extrusion temperature is further increased to 500 °C, the average grain sizes are 8.83 μm, 18.58 μm and 22.46 μm at the extrusion speeds of 0.2 m/min, 3.2 m/min and 32 m/min, respectively.

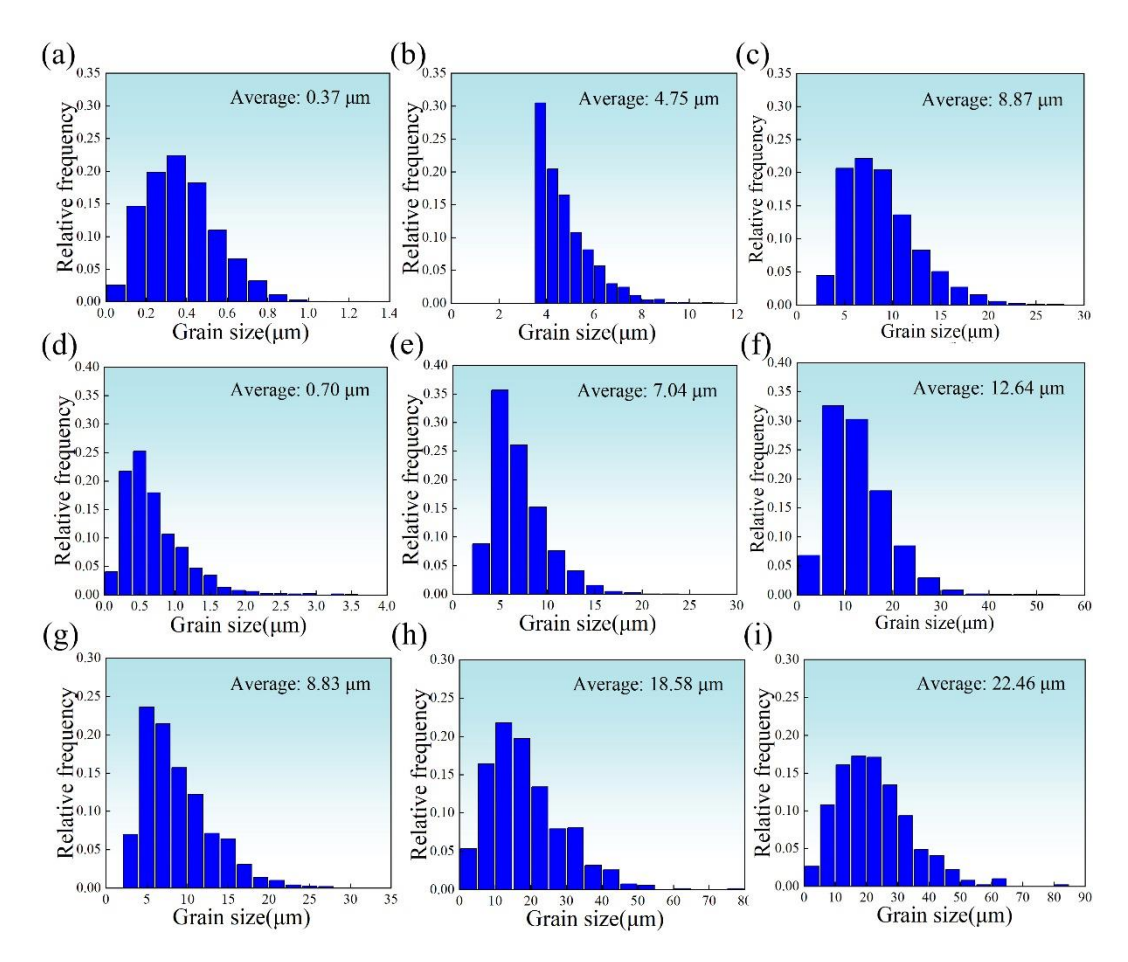


Fig. 5. Distribution of average grain size of recrystallized grains for rods under extrusion conditions: (a) 300 °C 0.2 m/min, (b) 300 °C 3.2 m/min, (c) 300 °C 32 m/min, (d) 400 °C 0.2 m/min, (e) 400 °C 3.2 m/min, (f) 400 °C 32 m/min, (g) 500 °C 0.2 m/min, (h) 500 °C 3.2 m/min, (i) 500 °C 32 m/min.

From Figs. 1-5, both the extrusion temperature and speed have significant effect on the microstructure evolution of Mg-2Zn-1Gd rods. With increasing the extrusion temperature, the area fraction of recrystallized grain increases, and the size of recrystallized grains become larger. During extrusion, the increase of extrusion temperature would promote dynamic recrystallization, and accelerates grain boundary migration. With the increase of extrusion speed, the size of recrystallized grains also increased. As shown in Fig. 6, evolution of grain size for the recrystallized grains with extrusion speed was a continuous process, indicating the temperature-dependent nature of the observed grain growth. Therefore, the dynamic recrystallization was promoted during high-speed extrusion.

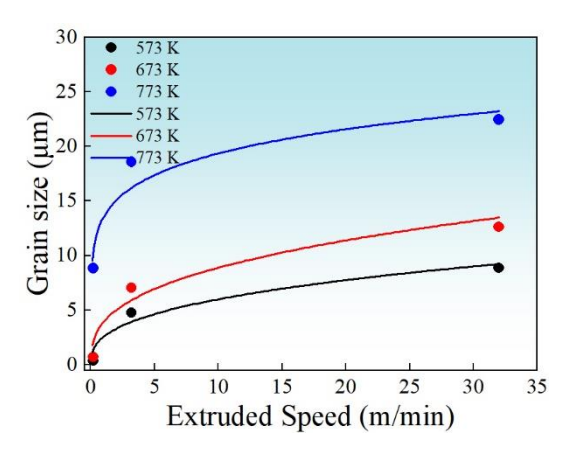


Fig. 6. Evolution of average grains with extrusion temperature and speed.

3.2. Mechanical properties of extruded Mg-2Zn-1Gd rods

Fig. 7 shows the engineering stress-strain curves of the extruded rods under tension and compression along the extrusion direction (ED). For tensile tests, the yield strength of the extruded rods generally decreases with the increasing of extrusion temperature or extrusion speed. At the extrusion temperature of 300 °C with extrusion speeds of 0.2 m/min, 3.2 m/min and 32 m/min, the yield strength are 324 MPa, 217 MPa and 190 MPa for extrusion speeds of 0.2 m/min, 3.2 m/min and 32 m/min, respectively. When the extrusion temperature is increased to 400 °C, the yield strength decreased to 253 MPa, 183 MPa and 179 MPa, respectively. Further increasing the temperature to 500 °C resulted in a further reduction in yield strength to 197 MPa, 162 MPa, and 158 MPa, respectively. In terms of elongation, the lowest values were observed at the highest extrusion temperature of 500 °C, with elongations of 10.51%, 10.25%, and 10.67% for extrusion speeds of 0.2 m/min, 3.2 m/min and 32 m/min, respectively. At lower extrusion temperatures (300 °C and 400 °C), the elongation varied significantly with extrusion speed. At 300 °C, the elongation was lowest at 0.2 m/min, about 10.2% and highest at 3.2 m/min, about 23.6%. Similarly, at 400 °C, the elongation was lowest at 0.2 m/min (14.6%) and highest at 3.2 m/min (23.0%). When the extrusion speed was increased to 32 m/min, the elongation is 20.1% and 15.4% at 300 °C and 400 °C, respectively. For compression tests, an increased extrusion temperature or speed generally results in a lower yield strength. At an extrusion temperature of 300 °C, the yield strength decreases from 214 MPa to 137 MPa and 99 MPa as the extrusion speed

increasing from 0.2 m/min, 3.2 m/min to 32 m/min. As the extrusion temperature increased to 400 °C, the yield strength decreased to 118 MPa, 86 MPa, and 63 MPa for the same extrusion speeds, and that is 73 MPa, 42 MPa, and 40 MPa at the extrusion temperature of 500 °C. The related mechanical properties for ED tension and ED compression are summarized at Tables 2 and Table 3, respectively.

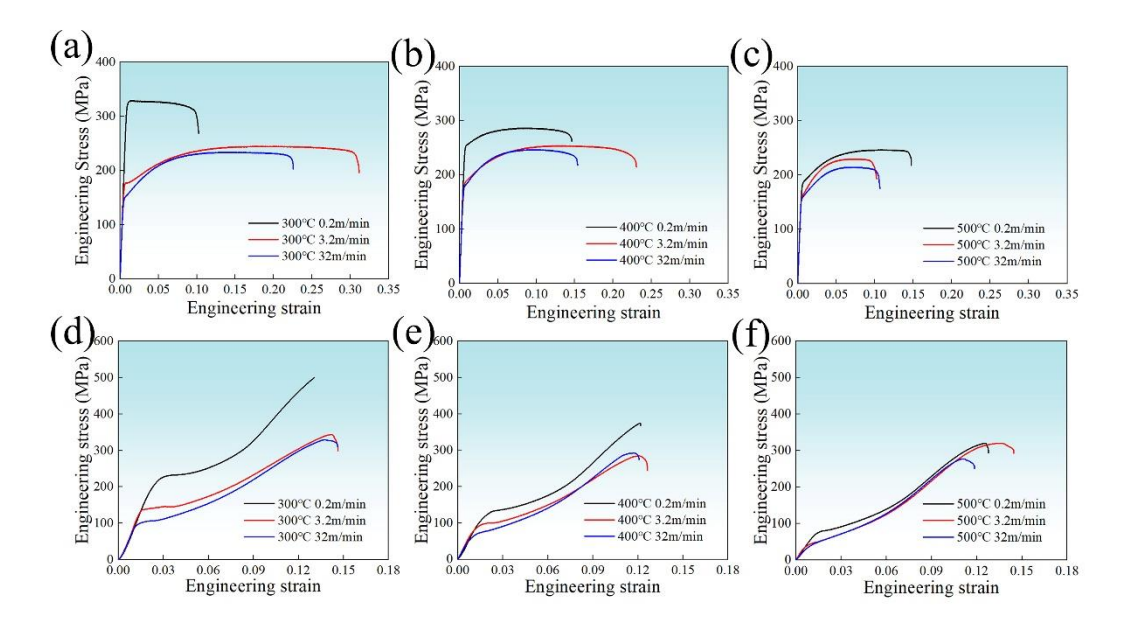


Fig. 7. Engineering stress-strain curves of Mg-2Zn-1Gd (wt.%) rod along ED direction (a-c) tension and (d-f) compression under different extrusion conditions.

Table 2. Tensile yield strength (YS), ultimate tensile strength (UTS) and elongation (EL) of extruded Mg-2Zn-1Gd rods under ED tension.

Samples	TYS(MPa)	UTS(MPa)	EL(%)
300°C 0. 2 m/min	323.6±2	329.3±1	10.2±3
300°C 3.2 m/min	216.6±2	285.8±3	23.6±1
300°C 32 m/min	190.4±1	273.9±2	20.1±3
400°C 0.2 m/min	253.2±3	286.2±4	14.6±1
400°C 3.2 m/min	183.4±3	253.8±3	23.0±1
400°C 32 m/min	178.5±2	246.5±3	15.4±1
500°C 0.2 m/min	197.5±3	253.5±4	10.5±2
500°C 3.2 m/min	162.1±3	229.6±2	10.3±2

500°C 32 m/min	157.7±2	214.4±4	10.7±2	_

Table 3. Compressive yield strength (YS), ultimate compressive strength (UCS) and compressive ductility (CD) of extruded Mg-2Zn-1Gd rods under ED tension.

Samples	CYS(MPa)	UCS(MPa)	CD(%)
300°C 0.2 m/min	213.5±4	499.8±4	13.1±3
300°C 3.2 m/min	137.1±3	343.4±4	14.6±1
300°C 32 m/min	98.6±3	329.5±3	14.6±1
400°C 0.2 m/min	117.8±3	374.6±5	12.2±1
400°C 3.2 m/min	86.4±4	284.7±4	12.6±1
400°C 32 m/min	62.6±1	292.6±1	12.1±1
500°C 0.2 m/min	73.5±4	320.5±5	12.8±1
500°C 3.2 m/min	41.5±2	320.5±3	14.5±1
500°C 32 m/min	40.3±1	277.6±3	11.9±1

From Fig. 7, the yield strength of the rods exhibit significant tension-compression asymmetry in the tensile and compressive strain-stress responses. The tension-compression asymmetry varies notably with extrusion temperatures and speeds. Fig. 8 shows the ratio of compressive to tensile yield strength under different extrusion conditions, providing a quantitative measure of tension and compression asymmetry. With the increase of extrusion temperature, the tension-compression asymmetry of the rods becomes more pronounced. It is found that at the extrusion temperature of 300 °C with extrusion speed of 0.2 m/min, the tension-compression asymmetry is the minimal, with a compressive-to-tensile yield strength ratio of approximately 0.66. In contrast, at the extrusion temperature of 500 °C and the extrusion speed of 3.2 m/min, the asymmetry reaches its maximum, with the ratio dropping to about 0.25.

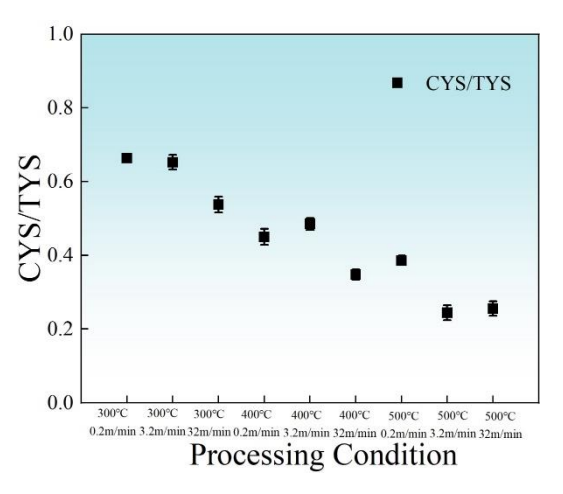


Fig. 8. Tensile-compression asymmetry in terms of yield strength under different extrusion conditions.

The stress- strain curves in Fig. 7 of all rods under ED tension show different shape compared to that under ED compression. That is, the stress- strain curves for all rods under ED tension are convex, while the stress- strain curves under ED compression show obvious concave (S-type) characteristics. Fig. 9 shows the work-hardening rate curves as a function of true strain under tension and compression for the rods prepared with different extrusion conditions. For ED-tension, the work-hardening rate decreased with an increase in tensile strain. At the extrusion temperature of 400 °C and 500 °C, the work hardening rate decreases with increasing the extrusion speed. However, at the extrusion temperature of 300 °C, the work hardening rate with an extrusion speed of 0.2 m/min is significantly lower than that with an extrusion speed of 3.2 m/min and 32 m/min. For ED-compression, single peak work hardening rate curve appear. That is, with the increasing of applied strain, the work hardening rate decreases first in the yield stage, from elasticity to plasticity, and then increases rapidly with the increase of strain, followed by a decrease again. When the extrusion temperature is 500 °C, the change of work hardening rate is not obvious with the increase of extrusion speed. On the contrary, at the extrusion temperature of 300 °C and 400 °C, the maximum work hardening rate decreases firstly and then increases slightly with the increase of extrusion speed.

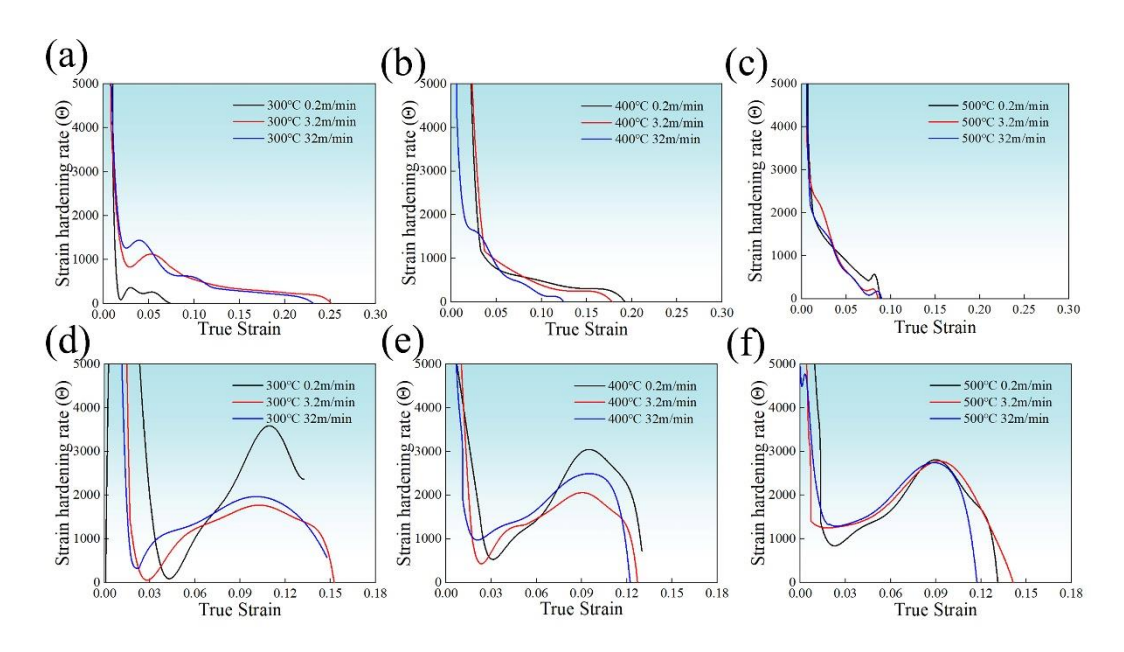


Fig. 9. Work-hardening rate curves of Mg-2Zn-1Gd (wt.%) rod along ED direction (a-c) tension and (d-f) compression under different extrusion conditions.

4. Discussion

4.1 Microstructure evolution with extrusion temperatures and speeds

From Figs. 1-2, both the extrusion temperature and extrusion speed impose significant effect on texture evolution of Mg-2Zn-1Gd rod. In order to quantitively analyze the texture evolution with extrusion parameters, the texture of extruded rods is divided into three typical groups, presented in Fig. 10a. That is, Texture I is within the position tilting from <0001> pole to < $\overline{1}2\overline{1}0$ > and < $01\overline{1}0$ > pole about 25°-70° of unit triangle, which is generally considered as RE texture [35, 36]. Texture II is within the position tilting from < $\overline{1}2\overline{1}0$ > pole to <0001> and < $01\overline{1}0$ > pole about 0-20° of unit triangle. Texture III is within the position tilting from < $01\overline{1}0$ > pole to <0001> and < $\overline{1}2\overline{1}0$ > pole about 0-20° of unit triangle. From Fig. 10, a higher extrusion temperature or speed generally contributes to the formation of Texture II and Texture III. For rod extruded at 300 °C with extrusion speed of 3.2 m/min, the area fraction of Texture I is about 42%. For rod extruded at 300 °C with extrusion speed of 32 m/min, the area fraction of Texture I slightly decreases to about 32%, while Texture I is dominant. For rod extruded at 500 °C with extrusion speed of 32 m/min, Texture II is dominant, and the area fraction of Texture II is about 38%. The texture evolution with extrusion

temperature is consistent with the results reported by Stanford et al.[24]. The results from this study further demonstrate that the extrusion speed also has significant effect on the texture evolution. That is, a lower extrusion speed contributes to the formation of RE-texture texture component, while a higher extrusion speed contributes to the formation of basal texture component. Which is rarely reported in the previous studies.

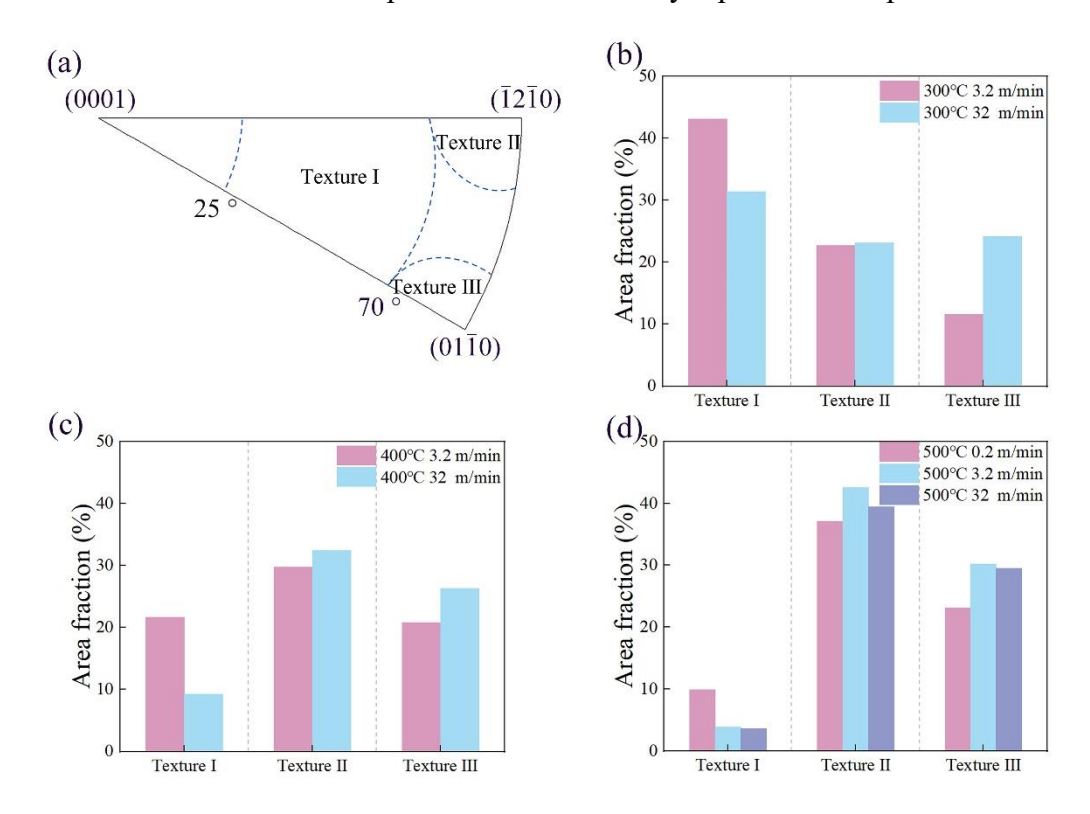


Fig. 10. Volume fraction of three typical orientation of Mg-2Zn-1Gd rods.

The mechanisms underlying the origin of the non-basal and basal textures of Mg alloys have been extensively studied, and the final texture characteristics were determined by both the texture evolution during grain nucleation and grain growth stages [37, 38]. From Fig. 1, the grain size of rods extruded at lower temperature and lower extrusion speed is much smaller than that extruded at higher temperature and higher extrusion speed. Herin the question arises, is it due to the instability of RE-texture during grain growth stage, that the basal texture has a growth advantage over the non-basal texture during high-temperature and high-speed extrusion, thus, leading to the occurrence of strong basal texture during extrusion at higher temperature and speed, and non-basal texture during extrusion at lower temperature and lower speed.

Comparison to statistic recrystallization, the mechanism on texture evolution during dynamic recrystallization is more complicated. During hot extrusion, both grain growth and plastic deformation occur in the recrystallized grains, and both could contribute to the visible texture evolution of Mg alloys. To identify the main contribution of grain growth and plastic deformation on texture evolution observed in this study during hot extrusion. The texture evolution of rod extruded at 300 °C with extrusion speed of 3.2 m/min during annealing is examined. The microstructure of rods after annealing at 400 °C for 30 min and 500 °C for 30 min are presented in Fig. 11. The average grain size is 8.12 μm and 17.17 μm for the rods annealed at 400 °C for 30 min and 500 °C for 30 min, respectively. For statistic recrystallization, the formation of RE texture of Mg-2Zn-1Gd rod have an advantage over the formation of $(10\overline{1}0)$ and $(11\overline{2}0)$ orientation during grain growth stage, and the area fraction of Texture I reach 47.9% and 46.1% at 400 °C and 500 °C, respectively. That is, the formation of RE texture has an advantage over the formation of basal texture during the growth advantage, which is well accepted of Mg-RE alloys [39, 40]. For Mg alloys, the activation of dislocations or twins in the recrystallized grains during hot extrusion would change the grain orientation. Wu et al. [41] investigated the texture evolution of Mg-1 wt.% Gd alloys during extrusion. It was shown that basal slip and prismatic slip occur of the $<2\overline{11}$ 1> DRX grains, then leading to a strong $<10\overline{1}0>$ fiber texture. Similar results have been reported on the hot-rolled Mg-1Gd alloy sheet by Basu et al. [42], it is reported that the plastic strain occurred in the recrystallized grains would contribute to the formation of strong ($10\overline{10}$) orientation. In this study, the effect of plastic deformation on texture evolution was examined in terms of kernel average misorientation (KAM) maps. For KAM maps, a higher KAM values generally represents a higher dislocation density [43]. Fig. 12 shows the KAM maps of rod extruded at 300 °C with speed of 3.2 m/min and rod extruded at 500 °C with speed of 32 m/min. From Fig. 12, Texture II and Texture III generally shows larger local misorientation than that of Texture I. It is clear that, comparing to RE texture, the grains of basal texture undergo larger plastic deformation during extrusion. It is considered that the addition of RE elements would increase the activity of non-basal slip [44, 45]. In addition, a higher temperature would also promote the activation of

pyramidal <c+a> slip due to the reduced ration of activation stress between pyramidal <c+a> slip and basal slip [46]. It is generally considered that the activation of pyramidal <c+a> slip would modify the basal texture of Mg alloys [47]. Li et al. [48] studied that the texture of Mg-13.9Gd-0.45Zr (wt.%) alloy at low strain, which is mainly composed of rare earth (RE) texture, and its C-axis direction is mainly parallel to the normal direction (ND). As the strain increases, the RE texture gradually transforms into the basal texture, and the C-axis direction is gradually parallel to the rolling direction (RD). This transformation is mainly due to the activation of pyramidal <c+a> slip and prismatic slip. Liu et al. [49] reported that AZ31 Mg alloy usually could generate a weak basal texture after direct extrusion and bending-shear deformation, due to that bending and shear deformation could promote the activities of non-basal slip. However, in this study, strong basal texture is observed for rods extruded at higher temperature with higher extrusion speed. Therefore, it is considered that the activation of non-basal slip during hot extrusion has limited effect on the texture evolution with extrusion parameters of Mg-2Zn-Gd rods.

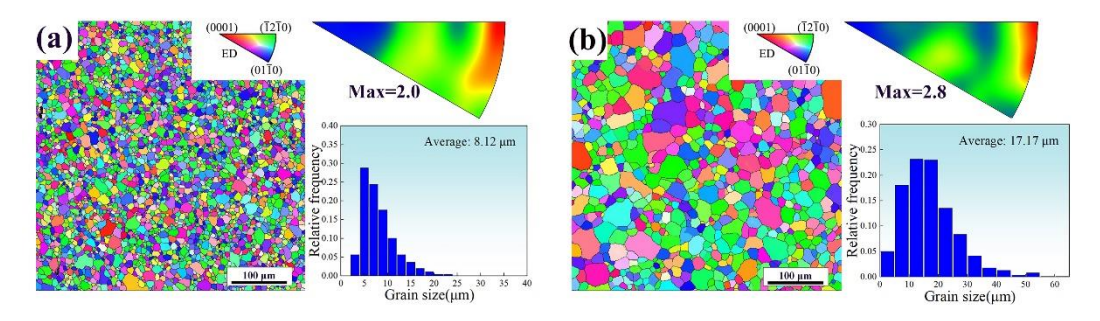


Fig. 11. EBSD IPF map, inverse pole figure and grain diameter distribution of fully recrystallized grains of Mg-Zn-Gd extruded rod at 300 °C 2.3 m/min after annealing (a) 400 °C for 30 min, (b) 500 °C for 30 min.

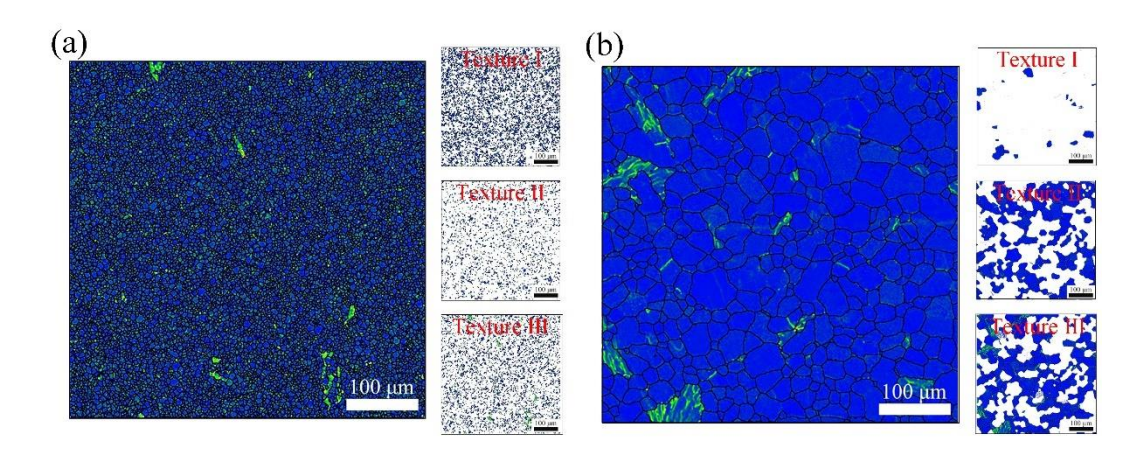


Fig. 12. Extrusion conditions of (a) 300°C 3.2m/min and 500°C 32m/min for different orientations of KAM distribution

It is reported that the extrusion temperature would have significant effect on the grain orientations at nucleation stage. For example, N. Stanford et al. [24] systematically studied the effect of extrusion temperature on the texture characteristics of Mg-1.5 wt.% Gd. It is found that $<1\overline{2}\overline{1}1>$ texture (RE texture) component would be dominant texture component of Mg-1.5 wt.% Gd, when the extrusion temperature is lower than 500 °C, while <0110> texture component would be the dominant texture component, when the extrusion temperature is higher than 500 °C. Further studies revealed that segregation of Gd atoms to grain boundaries plays an important role on modifying the grain orientation during nucleation stage at lower temperature. In this study, segregation of solute atoms to grain boundaries for rods extruded at 300 °C with speed of 0.2 m/min and extruded at 500 °C with speed of 0.2 m/min was exanimated by using energy-dispersive X-ray spectroscopy (EDS) in scanning transmission electron microscopy (TEM) mode (STEM-EDS). As shown in Fig. 13, the local concentration of both the Gd and Zn solutes at the grain boundary is higher than that of the matrix, which indicates an apparent solute segregation to grain boundary. Increasing the extrusion temperature to 500 °C decreases both the Gd and Zn concentration at the grain boundaries. Solute segregation to grain boundaries could retard recrystallization, which effectively increase the critical strain where dynamic recrystallization begins, then increase the orientation of nucleated grains. It is noted that dynamic

recrystallization is limited at lower temperature, and the formation of shear bands and twinning is promoted, which would also contribute to the nucleation of non-basal orientations. According to the nucleation characteristics, dynamic recrystallization can be divided into two main mechanisms: continuous dynamic recrystallization (CDRX) and discontinuous dynamic recrystallization (DDRX) [50, 51]. CDRX involves the recovery process of sub-grains formed by dislocation rearrangement. These sub-grains absorb dislocations in small angle grain boundaries (LAGB) and eventually transform into high angle grain boundaries (HAGB), which promotes the formation of new DRX grains. DDRX is realized by grain boundary migration, in which recrystallized grains nucleate and expand on zigzag HAGB; or with the increase of deformation, the new DDRX grains eventually form a large number of new- fine equiaxed grains around the original grains, showing a 'necklace' feature [52, 53]. From Fig. 1, CDRX is a more important mechanism at lower temperature, which contribute to the formation of RE texture. For Mg-RE alloys, it is considered that particles could provide heterogeneous nucleation sites for recrystallized grains with randomized orientations, thereby resulting in a weakened texture after recrystallization [54, 55]. Fig. 14 is the TEM-EDS diagram showing the distribution of second phase particles. The second phase particles are observed of the rods extruded at 300 °C, 400 °C and 500 °C, which are composited with Gd and Zn elements. Since the non-basal orientations have nucleation advantages for rods extruded at lower temperature, thus, it is considered the second phase particles have limited effect on the evolution of with extrusion parameters.

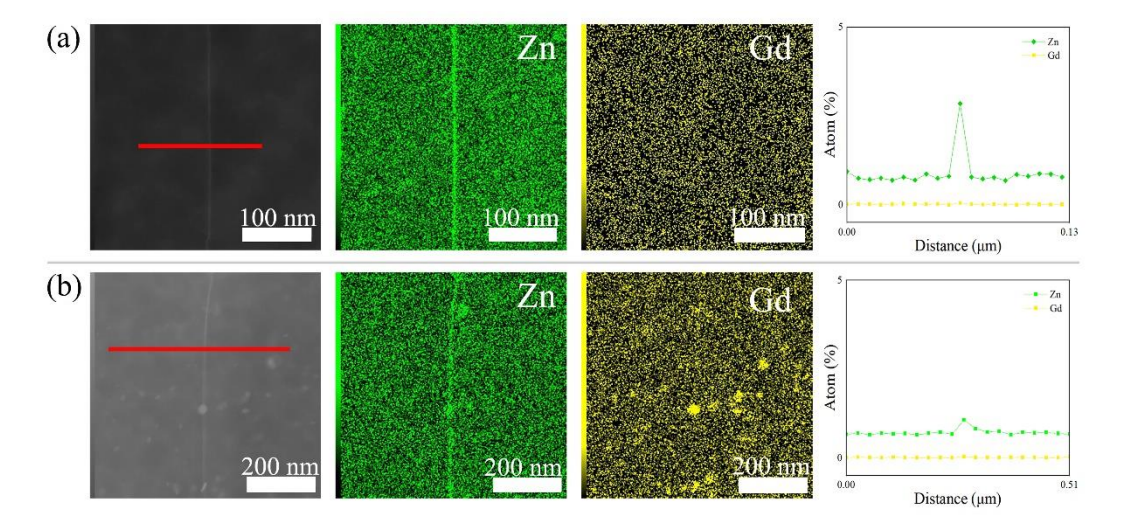


Fig. 13. Segregation of solute atoms at grain boundaries in Mg-2Zn-1Gd extruded rods under extrusion conditions at (a) 300 °C 0.2 m/min and (b) 500 °C 0.2 m/min.

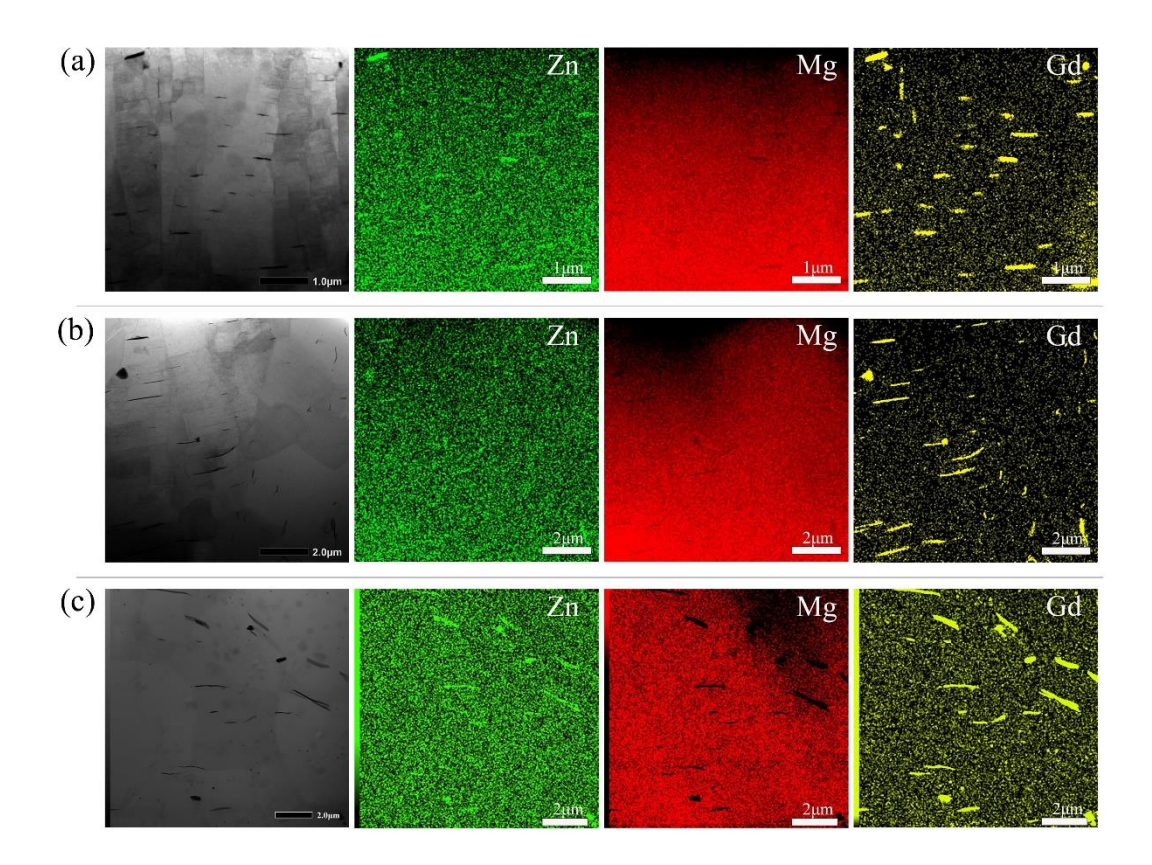


Fig. 14. TEM-EDS diagram of rods extruded with speed of 0.2 m/min at (a) 300 °C, (b) 400 °C, (c) 500 °C.

The above discussions are beneficial for explain the mechanism on the texture evolution with extrusion temperature and speed. As shown in Fig. 15, more solute atoms of Zn and Gd would segregate to grain boundaries of rods extruded at lower temperature with low extrusion speed. Grain boundary segregation of solute atoms would contribute to increase the critical strain for dynamic recrystallization, which could promote the formation of twins and shear bands, thus increasing the range of grain orientation after nucleation, and contributing to the formation of RE texture. For rods extruded at higher temperature and speed, basal slip would be activated in the recrystallized grains to accommodate the applied strain, which would contribute to the formation of strong basal texture.

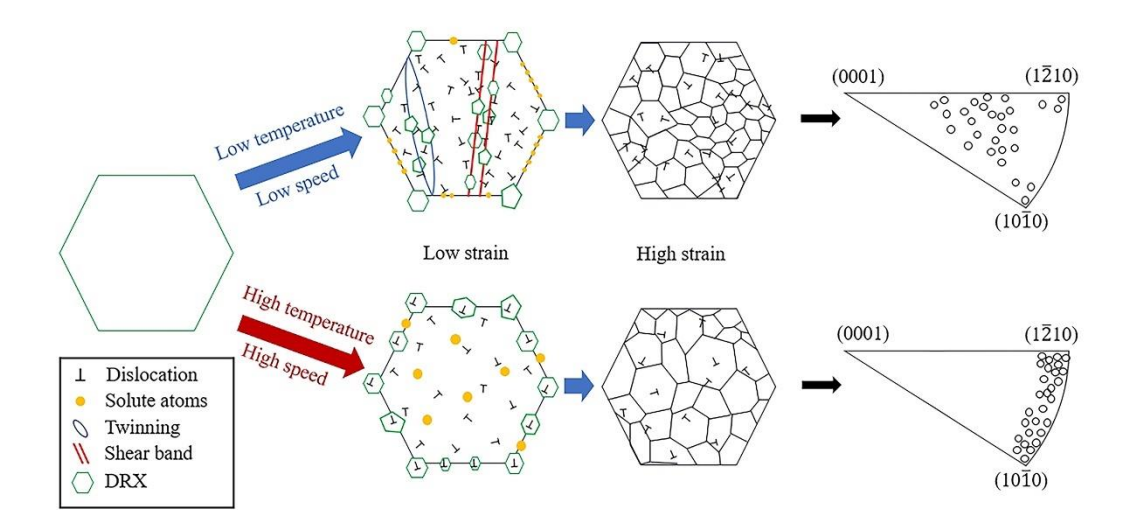


Fig. 15. Schematic showing the effect of extrusion parameters on texture evolution of Mg-2Zn-1Gd rod.

4.2 Effect of extrusion parameters on mechanical properties

From Fig. 7, the yield strength both under ED tension and ED compression would generally decreases with increasing extrusion temperature or speed. The changes of yield strength of Mg alloys are usually associated with evolution of grain size, dislocation density and texture with extrusion parameters.

It can be seen from Fig. 2 that high-density dislocations are observed of rod extruded at 300 °C with speed of 0.2 m/min. Due to the increase of extrusion temperature, the dynamic recrystallization is promoted, and the dislocations have sufficient thermal activation energy to interact and offset each other, so that the dislocation density in the grains decreases sharply with increasing the extrusion temperature and speed, which eventually leads to a lower yield strength.

The yield strength of the polycrystalline metals generally increases with the decrease of grain size. The evolution of strength with the average grain size can be quantitatively evaluated by the Hall-Petch relationship[56]:

$$\sigma_{v} = \sigma_{0} + k/\sqrt{d} \tag{1}$$

where σ_y is the yield stress, k is the Hall-Petch parameter, or the unpinning constant or "locking parameter", measuring the relative hardening contribution of grain/ phase boundaries, d is the average grain size, and σ_0 is the friction stress, denoting the

global crystal lattice resistance to dislocation movement (strength of the grain interior, represented by the strength of different phases present). The variation of the yield strength of the rods with (average grain size)^{-1/2} under tension and compression along ED are presented in Fig. 16. From Fig. 1, larger-deformed grains are observed in the rods extruded at 300 °C and 400 °C with speed of 0.2 m/min. It is very difficult to accurately determine the average grain size of these samples. Therefore, yield strength of the three rods under ED-tension and ED-compression are not considered in Fig. 16. From Fig. 16, the slope of the Hall-Petch relationship for ED tension is about 233.8 MPa µm^{1/2}. For ED compression, the Hall-Petch slope is about 373.9 MPa µm^{1/2}. It is apparent the slope for ED compression is higher than that of ED tension, which means that the grain size has a more significant effect on the yield strength during ED compression.

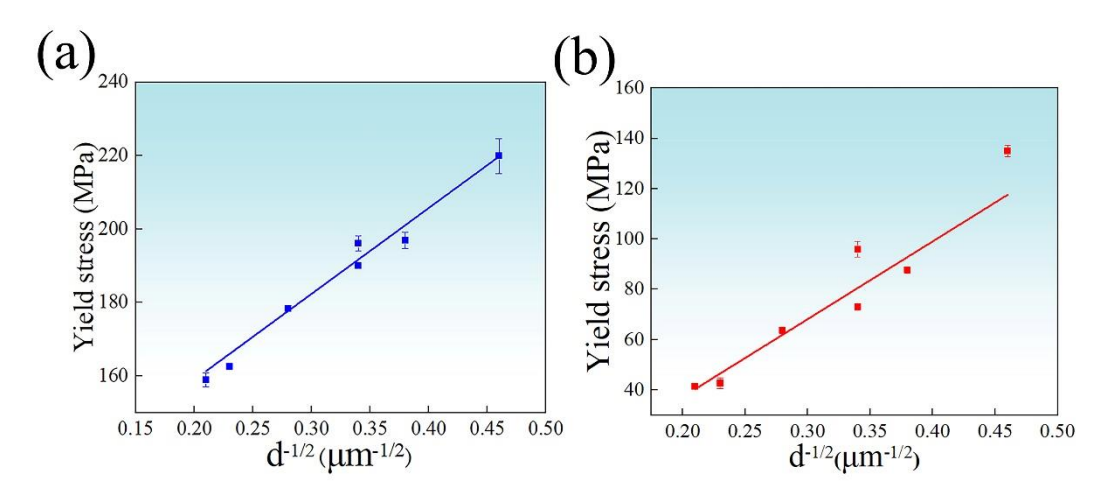


Fig. 16. Variation of the yield strength of the rods with (average grain size)^{-1/2} under (a) ED tension and (b) ED compression.

For Mg alloys, the texture evolution would also pose significant effect on strength [57, 58]. The variation of yield strength with texture could be quantitatively manifested by the activation stress of each grain. The activation stress is determined by both the grain orientation and critical resolved shear stress, as:

$$\sigma_a = CRSS/SF \tag{2}$$

where σ_a is the activation stress for each grain, *CRSS* is the critical resolved shear stress for each deformation mode [59], *SF* is the Schmid factor for each grain during

loading with specific direction[60]. During calculation, the activation stress for basal slip, prismatic slip and $\{10\overline{1}2\}$ twinning for a grain is calculated, then the mode with the lowest CRSS/SF is considered as the activated one for the grain. During calculation, the as-used CRSS ratio between prismatic slip, $\{10\overline{1}2\}$ twinning and basal slip is important, however, which is hardly to be determined experimentally for polycrystalline Mg alloys. It is considered that the CRSS ratio between prismatic slip and basal slip for AZ31 Mg alloys is about 2-5:1 [61, 62]. The addition of RE elements would reduce the CRSS ratio between non-basal slip and basal slip [63, 64]. Xu et al. [65] have successfully explained the effect of texture on the Hall-Petch relation of Mg-2Zn-1Gd (wt.%) Plate with a CRSS ratio of 1.5:1:1 for prismatic slip: {1012} twinning: basal slip. In addition, Zhang et al. [66] successfully revealed the effect of texture on mechanical properties of Mg-Zn-Gd alloys with a same CRSS ratio of 1.5: 1: 1 for prismatic slip: $\{10\overline{1}2\}$ twinning: basal slip. According to the previous studies, the CRSS ratio of 1.5: 1: 1 for prismatic slip: $\{10\overline{1}2\}$ twinning: basal slip is used in this study. As shown in Figs. 17-18, for ED tension, the activation stress of each grain for all the rods is in the range of $20 \sim 40$ MPa, and the average activation stress for each rod generally increases with increasing extrusion temperature and speed. For rods extruded at 300 °C with speed of 3.2 m/min, the average activation stress is about 29.5 MPa, which would increase to 32.0 MPa as increasing the extrusion temperature and speed to 500 °C and 32 m/min, respectively. For ED compression, the activation stress of the grain orientation of all rods varies mainly in the range of $20 \sim 50$ MPa, and the average activation stress of each rod would slightly decrease with increasing the extrusion temperature and speed. The average activation stresses for rod extruded at 300 °C with speed of 3.2 m/min is 23.6 MPa, which would slightly decrease to 22.7 MPa for rod extruded at 500 °C with speed of 32 m/min.

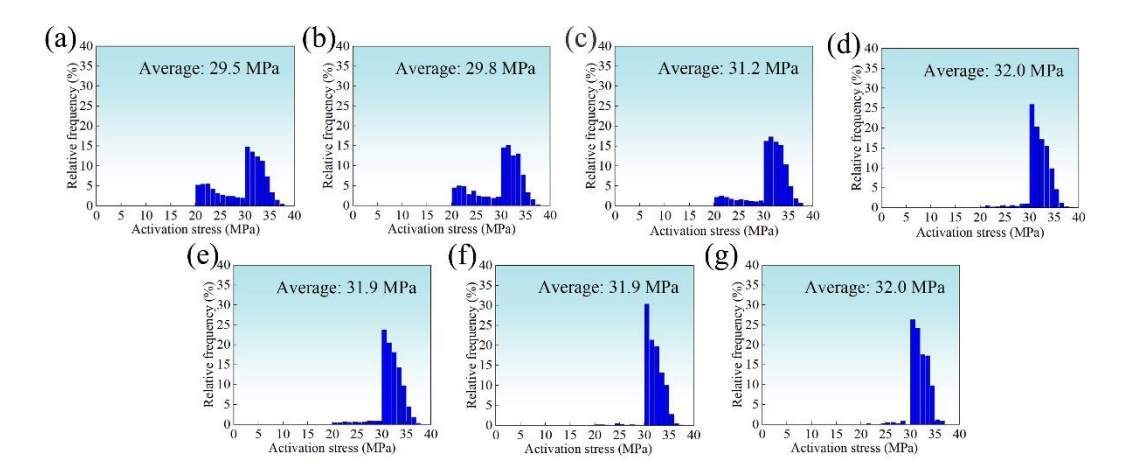


Fig. 17. Distribution of activation stress of Mg-2Zn-1Gd rods of 300 °C 3.2 m/min, 300 °C 32 m/min, 400 °C 3.2 m/min, 400 °C 32 m/min, 500 °C 0.2 m/min, 500 °C 3.2 m/min, and 500 °C 32 m/min under (a-g) ED tension.

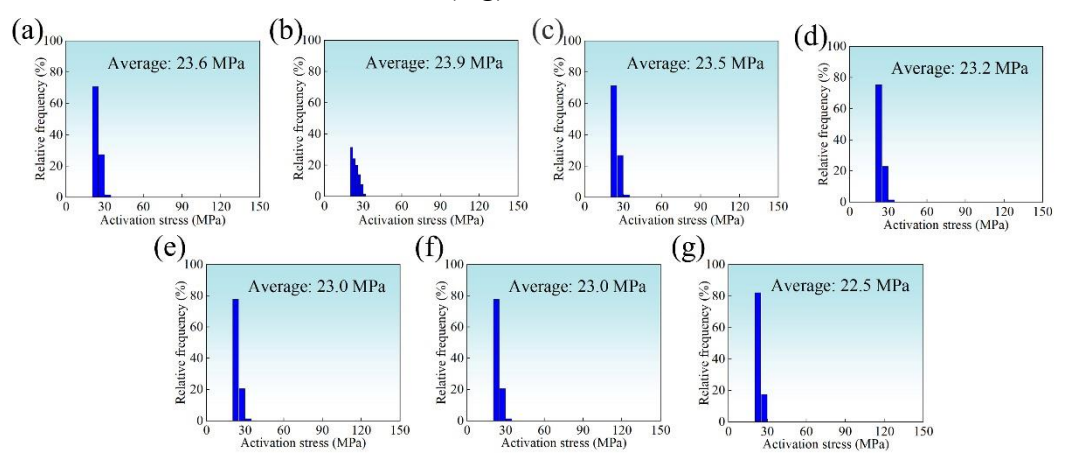


Fig. 18. Distribution of activation stress of Mg-2Zn-1Gd rods of 300 °C 3.2 m/min, 300 °C 32 m/min, 400 °C 3.2 m/min, 400 °C 32 m/min, 500 °C 0.2 m/min, 500 °C 3.2 m/min, and 500 °C 32 m/min under (a-g) ED compression.

In order to further analyze the effect of extrusion parameters on mechanical properties, the relative fraction of activated deformations for each rod under ED tension and ED compression are calculated and listed in Tables 4 and 5, respectively. For ED tension, prismatic slip is the main deformation mode, and a portion of basal slip is observed for each rod, while the fraction of basal slip and prismatic slip would vary with extrusion parameters. Generally, increasing the extrusion temperature or speed would increase the fraction of prismatic slip [67, 68]. For rod extruded at 300 °C with speed of 3.2 m/min, the fraction of basal slip and prismatic slip is 43.2% and 56%,

respectively. While, the fraction of prismatic slip would increase to 75.6%, as increasing the extrusion temperature to 400 °C. When the extrusion temperature is increased to 500 °C, the proportion of prismatic slip at 0.2 m/min, 3.2 m/min and 32 m/min is 88.9%, 95.7% and 94.8%, respectively. For ED compression, $\{10\overline{1}2\}$ twinning is the dominant deformation modes for all the rods. Basal slip could be activated in large amount for rods extruded at lower temperature and speed, while the fraction of basal slip would decrease as increasing the extrusion temperature and speed, and the fraction of basal slip would decrease to about 3.1% for rod extruded at 500 °C with speed of 32 m/min. According to the previous studies, the activated deformation modes and the activation stress for each grain of Mg alloys are mainly determined by the angle (θ) between loading direction and c-axis of the grain [51, 69]. In this study, the variation of activation stress and activated deformation mode with θ for ED tension and ED compression are calculated and presented in Fig. 19. For ED tension, prismatic slip would be the activated mode for θ within the range of 74-90°, basal slip would be the activated mode for θ within the range of 25-74°, and $\{10\overline{1}2\}$ twinning would be the activated mode for θ within the range of 0-25°. For ED compression, basal slip and $\{10\overline{1}2\}$ twinning would be the activated mode for θ within the range of 0-71° and 71- 90°, respectively. The relative frequency of θ for recrystallized grains are presented in Fig. 19c. It is observed that, the θ would be a wide range of 60-90° for rods extruded at lower temperature and speed, which would contribute to the activation of basal slip both under ED tension and ED compression, thus, resulting in a lower activation stress. For rods extruded at higher temperature with higher extrusion speed, i.e., rods extruded at 400 °C with speed of 32 m/min, at 500 °C with speed of 0.2 m/min, at 500 °C with speed of 3.2 m/min, at 500 °C with speed of 32 m/min, θ values are in a narrow range of 80-90°, due to the formation of strong basal texture, which would lead to the activation of prismatic slip under ED tension, thereby, resulting in a higher activation stress. While, for ED compression, these orientations would promote the activation of $\{10\overline{1}2\}$ twinning. The CRSS value of $\{10\overline{1}2\}$ twinning is similar to basal slip, and, the effect of texture on the average activation stress for rods under ED compression is limited. Thus, a higher tension-compression asymmetry is observed for

rods extruded at higher temperature and speed, as shown in Fig. 8. According to the above results, all the evolution of dislocation density, grain size and texture contribute to variation of yield strength of Mg-2Zn-1Gd rods with extrusion parameters. Increasing the extrusion temperature and speed would increase the grain size, while reduce dislocation density, both would contribute to a lower yield strength for rods extruded at higher temperature and speed. As shown in Fig. 16, the Hall-Petch slope for ED compression is much higher than that for ED tension. Therefore, efficiency of grain boundary strengthening for ED compression is much higher than that for ED tension, which would lead to a significantly lower yield strength for ED compression for rods extruded at higher temperature and speed, thereby, resulting in a higher tensioncompression asymmetry at higher temperature and speed. The effect of texture on the variation of yield strength with extrusion parameters could be summarized as follow. For ED tension, the activation of prismatic slip is promoted for rods extruded at higher temperature and speed due to the formation of strong basal texture, which would result in the higher activation stress for each, then, contributing to the higher yield strength. For ED compression, although, the relative fraction of basal slip and $\{11\overline{2}0\}$ twinning would vary with extrusion parameters, the effect of texture on yield strength is limited due to the small difference of CRSS value between basal slip and $\{11\overline{2}0\}$ twinning. In addition, the evolution of texture would also contribute the higher tension-compression asymmetry for rods extruded at higher temperature and speed, due to the different dependence of activated deformation modes and its activation stress on texture under ED tension and ED compression.

Table 4. Fraction of basal slip, prismatic slip, and $\{10\overline{1}2\}$ twinning under ED-tension.

Samples	Basal	Prismatic	Twinning
300 °C 3.2 m/min	43.2%	56.0%	0.8%
300 °C 32 m/min	40.0%	59.9%	0.1%
400 °C 3.2 m/min	24.1%	75.6%	0.2%
400 °C 32 m/min	11.2%	88.7%	0.1%
500 °C 0.2 m/min	10.9%	88.9%	0.2%

500 °C 3.2 m/min	4.1%	95.7%	0.2%
500 °C 32 m/min	5.2%	94.8%	0.1%

Table 5. Fraction of basal slip, prismatic slip, and $\{10\overline{1}2\}$ twinning under ED-compression.

Samples	Basal	Prismatic	Twinning
300 °C 3.2 m/min	34.6%	0	65.4%
300 °C 32 m/min	31.3%	0	68.7%
400 °C 3.2 m/min	16.8%	0	83.2%
400 °C 32 m/min	4.9%	0	95.1%
500 °C 0.2 m/min	6.4%	0	93.6%
500 °C 3.2 m/min	1.8%	0	98.2%
500 °C 32 m/min	3.1%	0	96.9%

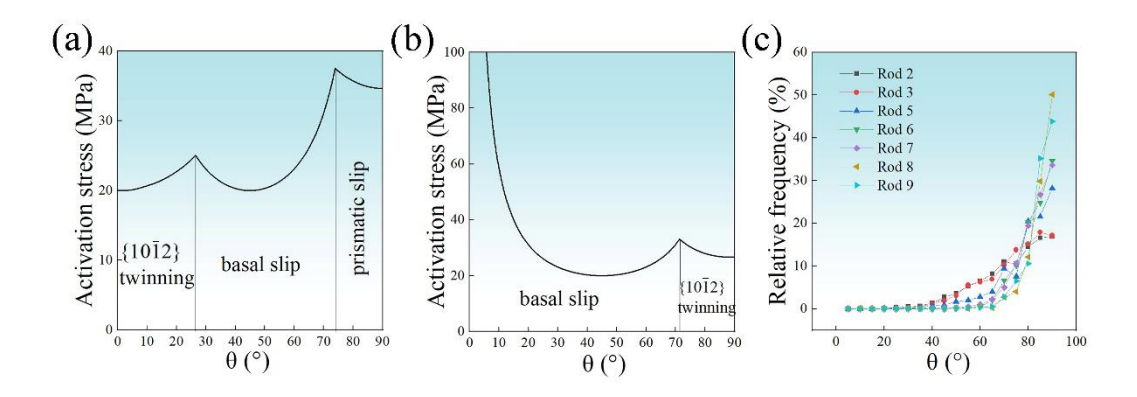


Fig. 19. Variation of activated deformation mode and activation stress with θ during (a) ED tension and (b) ED compression, and (c) distribution of θ value.

From Fig. 9, the hardening behavior for ED tension are significantly different to that for ED compression. For ED tension, the strain hardening rate of all rods continuously decreases with applied strain after the elastic-plastic transition. For ED compression, three distinguishable stages are observed for each rod after the elastic-plastic transition, that is, the strain hardening rate decrease with applied strain after the elastic-plastic transition (stage I), then rapidly increases with strain (stage II), and

flowed by a decrease in strain hardening rate again (stage III). Generally, the strong influence of texture on strain hardening behavior is related to the relative activities of slips and $\{10\bar{1}2\}$ twinning. It is reported that a continuous decrease of hardening rate with applied strain would occur when deformation is mainly accommodated by slips, while the presence of single-peak strain hardening with three stages is related to the activation of $\{10\bar{1}2\}$ twinning in large amount [70-72]. From Table 4, prismatic slip and basal slip would be the dominant deformation for all rod under ED tension, which would contribute to the continuous decrease of strain hardening rate. For ED compression, a higher portion of $\{10\bar{1}2\}$ twinning is observed for all rods, thus, which contributes to the rapid hardening. It is noted that the activation of $\{10\bar{1}2\}$ twinning is promoted for rods extruded at higher temperature and speed (i.e., rods extruded at 400 °C with speed of 32 m/min, at 500 °C with speed of 0.2 m/min, at 500 °C with speed of 3.2 m/min, at 500 °C with speed of 32 m/min), thus, these rods generally have higher peak values of strain hardening rate than the rods extruded at lower temperature and speed with fully recrystallized grains.

5. Conclusion

In this study, the extrusion temperature and speed demonstrated a significant impact on texture characteristics and mechanical properties of the extruded Mg-2Zn-1Gd rods. The main conclusions are as follows:

- (1) The yield strength and ultimate tensile strength generally decreases with increasing extrusion temperature and speed. When the rod extruded at 300 °C with extrusion speed of 3.2 m/min, the alloy exhibits the best combination of tensile strength and elongation, with a tensile strength of 285.8 MPa and an elongation of 23.6%, along with the optimal yield anisotropy.
- (2) The evolution of dislocation density, grain size and texture contribute to variation of yield strength of Mg-2Zn-1Gd rods with extrusion parameters. The decrease of dislocation density and grain growth with increasing extrusion temperature and speed would result in a lower stress. The Hall-Petch slope is larger under ED compression than that under ED tension, which indicates that the increase in grain

size has a greater influence on the strength, resulting in a more pronounced decrease in strength under ED compression. In addition, the formation of strong basal texture would contribute to a higher activation stress for rod extruded with higher temperature and speed under ED tension, however, which is limited under ED compression.

(3) The texture characteristics of Mg-2Zn-1Gd alloys changed significantly with the extrusion conditions. The formation of RE texture components is favored for rods extruded at lower temperature and speed, whereas the formation of basal texture components is favored as increasing the extrusion temperature and speed. The formation of RE texture for rods extruded at lower temperature and speed is related to the segregation of solute atoms at grain boundaries, which would contribute to increase the critical strain for dynamic recrystallization, thus increasing the range of grain orientation after nucleation.

Acknowledgements:

This work was financially supported by National Natural Science Foundation of China (52301151 and 52401151), Key R&D Projects of Jiangxi Province (20243BBG71024), Jiangxi Provincial Natural Science Foundation (20232BAB214002), Natural Science Foundation of Jiangsu Province (Nos. BK20232025 and BK20243005), Jiangxi Province Ganpo Juncai Support Program (20232BCJ23093, 20242BCE50038), Jiangxi Academy of Sciences (2024TJPT001). National Natural Science Foundation of China (52125505).

References

- [1] T.C. Xu, Y. Yang, X.D. Peng, J.F. Song, F.S. Pan, Overview of advancement and development trend on magnesium alloy, J. Magnes. Alloy. 7(3) (2019) 536-544. https://10.1016/j.jma.2019.08.001. [2] M. Jiang, C. Xu, T. Nakata, H. Yan, R. Chen, S. Kamado, Rare earth texture and improved ductility in a Mg-Zn-Gd alloy after high-speed extrusion, Mater. Sci. Eng. A. 667 (2016) 233-239. https://10.1016/j.msea.2016.04.093.
- [3] X.D. Huang, L. Wang, Y. Zhou, G.J. Huang, Y.C. Xin, Y. Cao, W. Li, S.H. Xiang, On the planar anisotropy of ductility in a dilute Mg-Zn-Gd alloy, Mater. Sci. Eng., A-Struct 894 (2024) 19.https://10.1016/j.msea.2024.146203.
- [4] Y.Z. Xing, J.B. Luo, Q.J. He, Y. Cheng, Y.C. Xin, An Mg-1Zn-1Cu-xCe alloys with both high ductility and high thermal conductivity, J. Alloys Compd. 1025 (2025).https://10.1016/j.jallcom.2025.180247.
- [5] X.N. Meng, D.T. Zhang, W.W. Zhang, C. Qiu, D.L. Chen, Achieving high damping capacity and strength simultaneously in a high-zinc aluminum alloy via melt spinning and hot extrusion, Mater. Sci. Eng., A-Struct 833 (2022).https://10.1016/j.msea.2021.142376.
- [6] T. Tamura, M.J. Li, K. Takahashi, E. Inoue, Improved solidification structures and mechanical properties of Al-20 wt% Sn alloys processed by an electromagnetic vibration technique, Mater. Sci. Eng., A-Struct 862 (2023).https://10.1016/j.msea.2022.144416.
- [7] U.M. Chaudry, Y. Noh, G. Han, R. Jaafreh, T.S. Jun, K. Hamad, Effect of CaO on structure and properties of AZ61 magnesium alloy, Mater. Sci. Eng., A-Struct 844 (2022).https://10.1016/j.msea.2022.143189.
- [8] A. Koushki, A. Jalali, N. Rasooli, A. Heydarinia, A. Geranmayeh, M.S. Mehranpour, H. Shahmir, Strength-ductility synergy in a wrought AZ80 magnesium alloy by microstructure engineering, Mater. Sci. Eng., A-Struct 889 (2024). https://10.1016/j.msea.2023.145764.
- [9] Z.R. Zeng, N. Stanford, C.H.J. Davies, J.F. Nie, N. Birbilis, Magnesium extrusion alloys: a review of developments and prospects, Int. Mater. Rev. 64(1) (2019) 27-62.https://10.1080/09506608.2017.1421439.
- [10] Y. Chen, R. Zhang, T. Zhou, L. Hu, J. Tu, L.X. Shi, Y. Zhi, L.W. Lu, Q. Chen, B.H. Liao, L. Liu, W.J. Ge, J. Xiao, M.B. Yang, Influence of Extrusion Speed on the Microstructure Evolution, Interface Bonding and Mechanical Response of Mg MB26/Al 7075 Composite Rod, Acta Metall. Sin.-Engl. Lett. 32(2) (2019) 253-262. https://10.1007/s40195-018-0838-x.
- [11] K. Zhang, J.H. Zheng, C. Hopper, C.Y. Sun, J. Jiang, Enhanced plasticity at cryogenic temperature in a magnesium alloy, Mater. Sci. Eng., A-Struct 811 (2021).https://10.1016/j.msea.2021.141001.
- [12] H. Moshaver, M.H. Sabzevar, M. Mazinani, M. Mahmoudi, Effect of bismuth on microstructure, mechanical properties and fracture behavior of AZ magnesium alloys, Mater. Sci. Eng., A-Struct 854 (2022).https://10.1016/j.msea.2022.143676.
- [13] B. Guan, L. Wang, Y.C. Xin, P.D. Wu, J. Xu, X.X. Huang, Q. Liu, Double-peak strain hardening behavior of Mg-1.2 wt. %Y alloy, Int. J. Plast. 179 (2024) 15.https://10.1016/j.ijplas.2024.104041.
- [14] T. Nakata, C. Xu, K. Sugiya, Y. Yoshida, K. Yoshida, L. Geng, S. Kamado, Microtexture-induced anomalous anisotropic tensile behavior in Mg-Al-Zn alloy sheet, Mater. Sci. Eng., A-Struct 840 (2022).https://10.1016/j.msea.2022.143002.
- [15] S.P. Kanti, R. Kumar, S.K. Panigrahi, B.N. Sahoo, Effect of rolling reduction on microstructure and tension-compression yield asymmetry of rolled AZ31 magnesium sheet, Mater. Sci. Eng., A-

- Struct 903 (2024).https://10.1016/j.msea.2024.146683.
- [16] J.F. Deng, J. Tian, Y.Y. Chang, Y.C. Zhou, W. Liang, J.Y. Ma, The role of {10-12} tensile twinning in plastic deformation and fracture prevention of magnesium alloys, Mater. Sci. Eng., A-Struct 853 (2022). https://10.1016/j.msea.2022.143678.
- [17] K. Frydrych, T. Libura, Z. Kowalewski, M. Maj, K. Kowalczyk-Gajewska, On the role of slip, twinning and detwinning in magnesium alloy AZ31B sheet, Mater. Sci. Eng., A-Struct 813 (2021).https://10.1016/j.msea.2021.141152.
- [18] P. Ye, C. Yang, Z. Li, S. Bao, Y. Sun, W. Ding, Y. Chen, Texture and High Yield Strength of Rapidly Solidified AZ31 Magnesium Alloy Extruded at 250° C, Materials 16(8) (2023) 2946.https://10.3390/ma16082946.
- [19] E. Chandiran, Y. Ogawa, R. Ueji, A. Singh, H. Somekawa, T. Ohmura, Activation of non <a> type dislocation in near <0001>-oriented Mg by Sc addition, Mater. Sci. Eng., A-Struct 890 (2024). https://10.1016/j.msea.2023.145927.
- [20] S. Sisodia, S. Jananandhan, V.K. Pakki, C. Konkati, A. Chauhan, Towards reducing tension-compression yield and cyclic asymmetry in pure magnesium and magnesium-aluminum alloy with cerium addition, Mater. Sci. Eng., A-Struct 886 (2023).https://10.1016/j.msea.2023.145672.
- [21] R.K. Mishra, A.K. Gupta, P.R. Rao, A.K. Sachdev, A.M. Kumar, A.A. Luo, Influence of cerium on the texture and ductility of magnesium extrusions, Scr. Mater. 59(5) (2008) 562-565. https://10.1016/j.scriptamat.2008.05.019.
- [22] R.K. Mishra, A. Brahme, R.K. Sabat, L. Jin, K. Inal, Twinning and texture randomization in Mg and Mg-Ce alloys, Int. J. Plast. 117 (2019) 157-172. https://10.1016/j.ijplas.2019.03.001.
- [23] G.M. Lee, S.H. Park, Underlying mechanisms of variation in yield asymmetry and strain hardening behavior of extruded pure Mg with Gd addition, J. Magnes. Alloy. 11(6) (2023) 2165-2181.https://10.1016/j.jma.2022.09.008.
- [24] N. Stanford, M. Barnett, The origin of "rare earth" texture development in extruded Mg-based alloys and its effect on tensile ductility, Mater. Sci. Eng. A. 496(1-2) (2008) 399-408. https://10.1016/j.msea.2008.05.045.
- [25] A.D. Mansoor, W.B. Du, Z.J. Yu, K. Liu, N. Ding, J.J. Fu, F. Lou, S.B. Li, Improved mechanical performance of double-pass extruded Mg-Gd-Er-Zr alloys with various rare earth contents, Mater. Sci. Eng., A-Struct 840 (2022).https://10.1016/j.msea.2022.142922.
- [26] Z.X. Zhang, S.X. Xia, X. Chen, L. Wang, Q.H. Wang, J. Xu, X. Qin, M. Ali, W.Q. Wang, W.Y. Huang, B. Jiang, Achieving ultra-high extrusion speed and strength-ductility synergy in a BAZ531 magnesium alloy via differential-thermal extrusion, Mater. Sci. Eng., A-Struct 923 (2025). https://10.1016/j.msea.2024.147687.
- [27] B. Kim, S.-M. Baek, J.G. Lee, S.S. Park, Enhanced strength and plasticity of Mg–6Zn–0.5 Zr alloy by low-temperature indirect extrusion, J. Alloys Compd. 706 (2017) 56-62. https://10.1016/j.jallcom.2017.02.206.
- [28] S.H. You, Y.D. Huang, K.U. Kainer, N. Hort, Recent research and developments on wrought magnesium alloys, J. Magnes. Alloy. 5(3) (2017) 239-253.https://10.1016/j.jma.2017.09.001.
- [29] J.W. Cha, S.C. Jin, S.H. Park, Influence of Ca addition on microstructural characteristics and mechanical properties of Mg-5Bi-3Al alloy extruded at extremely high speed, Mater. Sci. Eng., A-Struct 862 (2023).https://10.1016/j.msea.2022.144490.
- [30] N. Stanford, G. Sha, J. Xia, S.P. Ringer, M.R. Barnett, Solute segregation and texture modification in an extruded magnesium alloy containing gadolinium, Scr. Mater. 65(10) (2011)

- 919-921.https://10.1016/j.scriptamat.2011.08.012.
- [31] D.D. Zhang, C.M. Liu, S.N. Jiang, Y.H. Gao, Y.C. Wan, Z.Y. Chen, Effects of extrusion process on microstructure, precipitates and mechanical properties of Mg-Gd-Y-Zr-Ag alloys, Mater. Sci. Eng., A-Struct 856 (2022).https://10.1016/j.msea.2022.143990.
- [32] K.K. Verma, S. Kumar, S. Suwas, Evolution of microstructure and texture during hot rolling and subsequent annealing of the TZ73 magnesium alloy and its influence on tensile properties, Mater. Sci. Eng., A-Struct 821 (2021).https://10.1016/j.msea.2021.141480.
- [33] H. Zengin, Y. Turen, Effect of La content and extrusion temperature on microstructure, texture and mechanical properties of Mg-Zn-Zr magnesium alloy, Mater. Chem. Phys. 214 (2018) 421-430.https://10.1016/j.matchemphys.2018.04.110.
- [34] W.N. Zhang, H. Zhang, L.F. Wang, J.F. Fan, X. Li, L.L. Zhu, S.Y. Chen, H.J. Roven, S.Z. Zhang, Microstructure Evolution and Mechanical Properties of AZ31 Magnesium Alloy Sheets Prepared by Low-Speed Extrusion with Different Temperature, Crystals 10(8) (2020) 9.https://10.3390/cryst10080644.
- [35] G.Q. Wu, J.M. Yu, L.C. Jia, W.L. Xu, B.B. Dong, Z.M. Zhang, B.Y. Hao, Microstructure and Texture Evolution of Mg-Gd-Y-Zr Alloy during Reciprocating Upsetting-Extrusion, Materials 13(21) (2020).https://10.3390/ma13214932.
- [36] X.H. Pan, H. Yang, S. Yuan, Y.M. Jin, X.H. Chen, F.S. Pan, Uncovering the Role of Dynamic Recrystallization in <0001> Texture Formation during Hot Extrusion in Mg-Gd-Y-Zn Alloy, J. Alloys Compd. 1027 (2025).https://10.1016/j.jallcom.2025.180482.
- [37] J. Xu, B. Guan, X.J. Zhao, R. Fu, Q. Hu, C.Q. Liu, Strain Rate Dependence of Twinning Behavior in AZ31 Mg Alloys, Metals 13(11) (2023). https://10.3390/met13111882.
- [38] X.D. Huang, Y.C. Xin, Y. Cao, G.J. Huang, W. Li, A quantitative study on planar mechanical anisotropy of a Mg-2Zn-1Ca alloy, J. Mater. Sci. Technol 109 (2022) 30-48.https://10.1016/j.jmst.2021.07.051.
- [39] K. Hantzsche, J. Bohlen, J. Wendt, K.U. Kainer, S.B. Yi, D. Letzig, Effect of rare earth additions on microstructure and texture development of magnesium alloy sheets, Scr. Mater. 63(7) (2010) 725-730.https://10.1016/j.scriptamat.2009.12.033.
- [40] J.L. Wu, L. Jin, J. Dong, F.H. Wang, S. Dong, The texture and its optimization in magnesium alloy, J. Mater. Sci. Technol 42 (2020) 175-189. https://10.1016/j.jmst.2019.10.010.
- [41] W. Wu, L. Jin, Z. Zhang, W. Ding, J. Dong, Grain growth and texture evolution during annealing in an indirect-extruded Mg–1Gd alloy, J. Alloys Compd. 585 (2014) 111-119.https://10.1016/j.jallcom.2013.09.028.
- [42] I. Basu, T. Al-Samman, G. Gottstein, Shear band-related recrystallization and grain growth in two rolled magnesium-rare earth alloys, Mater. Sci. Eng., A-Struct 579 (2013) 50-56. https://10.1016/j.msea.2013.04.076.
- [43] M. Shenoy, J. Zhang, D.L. McDowell, Estimating fatigue sensitivity to polycrystalline Ni-base superalloy microstructures using a computational approach, FATIGUE FRACT ENG M 30(10) (2007) 889-904.https://10.1111/j.1460-2695.2007.01159.x.
- [44] L. Wang, Z. Huang, H. Wang, A. Maldar, S. Yi, J.-S. Park, P. Kenesei, E. Lilleodden, X. Zeng, Study of slip activity in a Mg-Y alloy by in situ high energy X-ray diffraction microscopy and elastic viscoplastic self-consistent modeling, Acta Mater. 155 (2018) 138-152. https://10.1016/j.actamat.2018.05.065.
- [45] D.D. Yin, C.J. Boehlert, L.J. Long, G.H. Huang, H. Zhou, J. Zheng, Q.D. Wang, Tension -

- compression asymmetry and the underlying slip/twinning activity in extruded Mg Y sheets, Int. J. Plast. 136 (2021).https://10.1016/j.ijplas.2020.102878.
- [46] A. Chapuis, J.H. Driver, Temperature dependency of slip and twinning in plane strain compressed magnesium single crystals, Acta Mater. 59(5) (2011) 1986-1994.https://10.1016/j.actamat.2010.11.064.
- [47] M. Jahedi, B.A. McWilliams, P. Moy, M. Knezevic, Deformation twinning in rolled WE43-T5 rare earth magnesium alloy: Influence on strain hardening and texture evolution, Acta Mater. 131 (2017) 221-232.https://10.1016/j.actamat.2017.03.075.
- [48] C. Li, J. Jin, H. Yan, Z. Shan, B. Liu, R. Chen, Non-basal slip induced rare earth texture evolution in Mg-14Gd-0.5 Zr (wt%) alloy during the traditional hot rolling, J. Alloys Compd. 994 (2024) 174737.https://10.1016/j.jallcom.2024.174737.
- [49] X.-Y. Liu, L.-W. Lu, K. Sheng, T. Zhou, Microstructure and texture evolution during the direct extrusion and bending—shear deformation of AZ31 magnesium alloy, Acta Metall. Sin. (Engl. Lett.). 32 (2019) 710-718.https://10.1007/s40195-018-0848-8.
- [50] B. Guan, Y.T. Wang, J.B. Li, Y. Zhang, H. Wang, Y.C. Xin, Comprehensive study of strain hardening behavior of CrCoNi medium-entropy alloy, J. Alloys Compd. 882 (2021).https://10.1016/j.jallcom.2021.160623.
- [51] Z.R. Zeng, Y.M. Zhu, S.W. Xu, M.Z. Bian, C.H.J. Davies, N. Birbilis, J.F. Nie, Texture evolution during static recrystallization of cold-rolled magnesium alloys, Acta Mater. 105 (2016) 479-494.https://10.1016/j.actamat.2015.12.045.
- [52] N. Ding, W.B. Du, S.B. Li, K. Liu, X. Du, Z.J. Yu, Strain rate dependence of dynamic recrystallization and texture evolution in hot compressed Mg-Gd-Er-Zr alloy, J. Magnes. Alloy. 13(1) (2025) 161-171.https://10.1016/j.jma.2023.10.006.
- [53] Q. Zhang, Q.A. Li, X.Y. Chen, J.X. Zhao, J. Bao, Z.Y. Chen, Dynamic precipitation and recrystallization mechanism during hot compression of Mg-Gd-Y-Zr alloy, J. Mater. Res. Technol-JMRT 15 (2021) 37-51.https://10.1016/j.jmrt.2021.08.013.
- [54] X.Y. Liu, L.W. Lu, K. Sheng, T. Zhou, Microstructure and Texture Evolution During the Direct Extrusion and Bending-Shear Deformation of AZ31 Magnesium Alloy, Acta Metall. Sin.-Engl. Lett. 32(6) (2019) 710-718. https://10.1007/s40195-018-0848-8.
- [55] Y.N. Lin, S.M. Wu, Y.X. Wang, H. Chen, G. Li, W.D. Xie, G.B. Wei, Y. Yang, X.D. Peng, Dynamic recrystallization mechanism of high-strength Mg-Gd-Y-Zn-Mn alloy by hot compression deformation, J. Mater. Res. Technol-JMRT 35 (2025) 2422-2433. https://lo.1016/j.jmrt.2025.01.160.
- [56] E. Hall, Variation of hardness of metals with grain size, Nature 173(4411) (1954) 948-949.https://10.1038/173948b0.
- [57] X.D. Huang, Y.C. Xin, Y. Cao, W. Li, G.J. Huang, X. Zhao, Q. Liu, P.D. Wu, Understanding the mechanisms of texture evolution in an Mg-2Zn-1Ca alloy during cold rolling and annealing, Int. J. Plast. 158 (2022). https://10.1016/j.ijplas.2022.103412.
- [58] I. Basu, T. Al-Samman, Triggering rare earth texture modification in magnesium alloys by addition of zinc and zirconium, Acta Mater. 67 (2014) 116-133. https://10.1016/j.actamat.2013.12.015.
- [59] A. Baczmanski, P. Kot, S. Wronski, M. Wróbel, M. Wronski, J. Pilch, M. Muzyka, K. Wierzbanowski, Y. Zhao, L. Le Joncour, M. François, B. Panicaud, Direct diffraction measurement of critical resolved shear stresses and stress localisation in magnesium alloy, Mater. Sci. Eng., A-Struct 801 (2021).https://10.1016/j.msea.2020.140400.

- [60] J.F. Nie, K.S. Shin, Z.R. Zeng, Microstructure, Deformation, and Property of Wrought Magnesium Alloys, METALL MATER TRANS A 51(12) (2020) 6045-6109. https://10.1007/s11661-020-05974-z.
- [61] L.Y. Zhao, C. Zhang, H.R. Yang, C.J. Yan, Y. Cheng, X.Q. Guo, Z.Y. Jin, Y.C. Xin, A comparative study on the different hardening on basal slip and prismatic slip mediated by pre-twins and dislocations of AZ31 alloys at room temperature and cryogenic temperature, J. Mater. Res. Technol-JMRT 36 (2025) 9100-9112.https://10.1016/j.jmrt.2025.05.121.
- [62] W.C. Zhang, J.Q. Pan, S.H. Wang, J.L. Yang, Texture weakening and grain refinement behavior of the extruded Mg-6.03Zn-0.55Zr alloy during hot plane strain compression, J. Mater. Res. Technol-JMRT 27 (2023) 3041-3053.https://10.1016/j.jmrt.2023.10.112.
- [63] C.Q. Liu, X.H. Chen, J. Chen, A. Atrens, F.S. Pan, The effects of Ca and Mn on the microstructure, texture and mechanical properties of Mg-4 Zn alloy, J. Magnes. Alloy. 9(3) (2021) 1084-1097.https://10.1016/j.jma.2020.03.012.
- [64] I.H. Jung, M. Sanjari, J. Kim, S. Yue, Role of RE in the deformation and recrystallization of Mg alloy and a new alloy design concept for Mg-RE alloys, Scr. Mater. 102 (2015) 1-6.https://10.1016/j.scriptamat.2014.12.010.
- [65] X. Jin, G. Yang, X. Xu, D. Shan, B. Guo, B. He, C. Fan, W. Xu, On the origin of non-basal texture in extruded Mg-RE alloys and its implication for texture engineering, J. Magnes. Alloy. (2024). https://10.1016/j.jma.2024.10.004.
- [66] P. Zhang, Y. Xin, L. Zhang, S. Pan, Q. Liu, On the texture memory effect of a cross-rolled Mg-2Zn-2Gd plate after unidirectional rolling, J. Mater. Sci. Technol 41 (2020) 98-104.https://10.1016/j.jmst.2019.05.076.
- [67] W. Wang, J.X. Liu, A.K. Soh, Crystal plasticity modeling of strain rate and temperature sensitivities in magnesium, Acta Mech. 230(6) (2019) 2071-2086. https://10.1007/s00707-019-2374-9.
- [68] W.Q. Tang, S.Y. Huang, S.R. Zhang, D.Y. Li, Y.H. Peng, Influence of extrusion parameters on grain size and texture distributions of AZ31 alloy, J. Mater. Process. Technol. 211(7) (2011) 1203-1209. https://10.1016/j.jmatprotec.2011.01.014.
- [69] B. Guan, J. Xu, R. Fu, S.Y. Xu, X. Li, Y.F. Jia, Q. Hu, Y.C. Xin, Significantly extending the gradient layer and mechanical properties of Mg alloys by texture optimization, Mater. Res. Lett. (2025). https://10.1080/21663831.2025.2514772.
- [70] X. Luo, X.N. Wang, Y.P. Xia, G.L. Wu, Y. Cheng, T.B. Yu, P.J. Yan, Y.C. Xin, X.X. Huang, On the microstructural origin of yield point phenomenon and high work-hardening response in fine-grained Mg-3Gd alloy, J. Mater. Sci. Technol 226 (2025) 290-301. https://10.1016/j.jmst.2024.12.008.
- [71] B. Guan, Y. Xin, X. Huang, P. Wu, Q. Liu, Quantitative prediction of texture effect on Hall–Petch slope for magnesium alloys, Acta Mater. 173 (2019) 142-152.https://doi.org/10.1016/j.actamat.2019.05.016.
- [72] P.D. Wu, X.Q. Guo, H. Qiao, S.R. Agnew, D.J. Lloyd, J.D. Embury, On the rapid hardening and exhaustion of twinning in magnesium alloy, Acta Mater. 122 (2017) 369-377.https://10.1016/j.actamat.2016.10.016.